2. ENERGY LOSS OF HIGH-VELOCITY IONS IN MATTER

By Wei-Kan Chu

2.1. Introduction

When high-velocity ions penetrate a material, they interact with the target atoms along their trajectories and lose energy to them by several mechanisms. One mechanism transfers energy from the moving ions to the target electrons through excitation and ionization of the target atoms. Another mechanism transfers energy from the ions to the target nuclei through momentum transfer.

Energy loss and scattering have been an important source of information on the constitution of atoms. Theoretical and experimental work on this subject have been going on since the beginning of the century. Information on energy loss is needed in many experiments in atomic and nuclear physics: to determine the energy and mass of a given nuclear reaction product in a cloud chamber or an emulsion, to correct the energy of an ion beam that has passed through thin windows or materials in a given experiment, to design radiation shielding, etc.

More recently, the various applications of ion beams in material study (for example, range, range distribution, and radiation damage in ion implantation; ion sputtering; ion backscattering; and ion-induced excitation) have led to further needs for knowledge of the energy loss of ions in matter. Most experimental work with ion beams requires information on energy loss. Such information, then, is basic to experimental physics.

This part is addressed to experimentalists who (1) want a general background on energy loss, (2) need energy loss information for their experiments, or (3) want to measure energy loss. With these three objectives in mind, we start with the general concepts of energy loss, a few theories, some experimental verification of theories as background material, some rules for interpolation and extrapolation, and a few references on existing compilations of information for those who need to use specific values of energy loss. In the last half of this part we emphasize various experimental methods of measuring energy loss, the trade-offs among them, and the accuracy and applicable region of each.

METHODS OF EXPERIMENTAL PHYSICS, VOL. 17

ISBN 0-12-475959-9

There have been many publications on ion beam penetration. Sigmund[1] has written an excellent review article on the subject, with a list of 219 papers and a good extraction of current theories and formulas. Andersen[2] has made a compilation of papers on experimental range and energy loss. He has assembled a bibliography containing over 800 titles, cross-indexed for species as related to projectiles as well as targets so that publications relevant to any ion–target combination can be retrieved easily.

2.2. General Concepts of Energy Loss

There are several energy loss mechanisms for moving ions in a target material:

(1) *Excitation and ionization.* This is the principal mechanism for the energy loss of ions at high velocities. Moving ions transfer their energies to the target electrons and thus promote some of the target atoms into excited or ionized states. Energy loss due to excitation and ionization is also called electronic energy loss, or inelastic energy loss.

(2) *Nuclear collisions.* This is the major mechanism for energy loss of projectiles at low velocities. Projectiles transfer their energies to the target nuclei by elastic collisions, and consequently the target atom recoils. Energy loss due to a nuclear collision is also called nuclear energy loss or elastic energy loss.

(3) *Generation of photons.* This mechanism is significant only at relativistic velocities. Projectiles emit photons because of deceleration in the medium (bremsstrahlung).

(4) *Nuclear reactions.* For certain very specific combinations of projectile, energy, and target, a nuclear reaction can be induced.

Here we concentrate on the first two of these mechanisms.

Microscopically, energy loss due to excitation, ionization, or nuclear motion is a discrete process. Macroscopically, however, it is a good assumption that the moving ions lose energy continuously. All we are concerned with here is the total collective effect of the energy attenuation during the penetration of ions into a given material. Individual effects due to a single collision are treated in separate chapters.

[1] P. Sigmund, *in* "Radiation Damage Processes in Materials" (*Proc. Radiat. Damage Processes Mater., Aleria, Corsica, France, August 27 to September 9, 1973*), pp. 3–118. Noordhoff, Leyden, 1975.

[2] H. H. Andersen, "Bibliography and Index of Experimental Range and Stopping Power Data." Pergamon Press, New York, 1977.

A good assumption, which has been implied so far, is that electronic energy loss and nuclear energy loss are not correlated, and therefore can be treated separately and independently. To measure energy loss, we must determine two quantities: the distance Δx that the ions traverse in the target, and the energy loss ΔE in this distance. The mass density ρ or the atomic density N are frequently combined with the distance, in the form $\rho\,\Delta x$ or $N\,\Delta x$, to express the amount of material per unit area or the number of atoms per unit area that the projectiles have traversed in losing energy ΔE to the target material. The atomic density N is related to the mass density ρ by Avogadro's number N_0 and to the mass number of the target M_2 by

$$N \equiv N_0\rho/M_2. \tag{2.2.1}$$

Energy loss can be expressed in several different ways. Some frequently used units are

$$\begin{aligned} dE/dx&: \quad \text{eV/Å, MeV/cm,} \\ dE/\rho\,dx&: \quad \text{eV/}(\mu\text{g/cm}^2)\text{, keV/}(\mu\text{g/cm}^2)\text{, MeV/}(\mu\text{g/cm}^2)\text{,} \\ dE/N\,dx&: \quad \text{eV/(atoms/cm}^2)\text{, eV-cm}^2. \end{aligned} \tag{2.2.2}$$

In the literature, and especially in some of the earlier experimental work, many different units derived from the above three forms have appeared. In many publications all three are called energy loss or dE/dx. One has to translate the units carefully when comparing one measurement to another.

Recently, most authors have adopted $dE/N\,dx$ (eV-cm^2) as the stopping cross section. Experimental physicists formerly used ϵ for this term, that is,

$$\epsilon \equiv \frac{1}{N}\frac{dE}{dx} \quad (\text{eV-cm}^2). \tag{2.2.3}$$

Theoretical physicists tend to prefer S, for example,

$$S \equiv \frac{\langle \Delta E \rangle}{N\,\Delta x} = \sum_i T_i P_i = \int T\,d\sigma, \tag{2.2.4}$$

where $\langle \Delta E \rangle$ is the average energy lost to a target of thickness $N\,\Delta x$, T_i the kinetic energy transferred to the ith electron with probability P_i, and the integral extends over all possible energy losses in individual collisions. The last term of Eq. (2.2.4) describes the cross section $d\sigma$ of the energy loss (stopping process), which therefore is called the stopping cross section. Thus Eqs. (2.2.3) and (2.2.4) have the same dimensions and the same meaning.

The advantage of using the stopping cross section (ϵ or S) rather than dE/dx is obvious. Especially in a systematic study, ϵ gives a description of energy loss on an atom-to-atom basis, which permits convenient extrapolation, whereas dE/dx changes for different materials, or even for the same material at different densities.

The earliest theoretical development on energy loss was done by Bohr.[3,4] His theory gives a quantitative account of the essential features of the process. Quantum-mechanical treatments later confirmed his analysis. Bethe[5–7] developed the theory further. Lindhard and coworkers[8–10] and Firsov[11,12] have contributed to the understanding of energy loss of ions at low velocity.

Figure 1 gives a schematic diagram of the proton-stopping cross section in silicon. The selection of projectile and target is arbitrary. Other selections will produce similar curves, with some differences in shape and scale. Some of the names and terms in Fig. 1 have not yet been defined or described here; they are presented in Fig. 1 for the purpose of relating each of the various theories to its region of applicability.

Figure 1 covers a very broad range of energies. It starts from a fraction of a kiloelectron volt to many gigaelectron volts. This curve has a peak at about 100 keV and a dip around 500 GeV. The increase in energy loss at relativistic velocities is due to photon emission, bremsstrahlung, and Cerenkov radiation. In this study we focus our attention on the nonrelativistic energy region.

In Fig. 1, the nuclear energy loss is small when compared to the electronic energy loss, even at very low energy. For example, according to Lindhard *et al.*[9,13] (LSS theory), nuclear stopping accounts for 2% of the total stopping for protons in silicon at 10 keV, and 16% for 1 keV. In studies of energy loss, therefore, nuclear energy loss can be ignored, especially for light ions at medium and high velocities. Nuclear collisions,

[3] N. Bohr, *Phil. Mag.* 25, (6) 10 (1913).
[4] N. Bohr, *Mat. Fys. Medd. Dan. Vid. Selsk.* 18, No. 8 (1948).
[5] H. A. Bethe, *Ann. Phys.* 5 (5), 325 (1930).
[6] H. A. Bethe, *Z. Phys.* 76, 293 (1932).
[7] H. A. Bethe, *Phys. Rev.* 89, 1256 (1953).
[8] J. Lindhard, *Mat. Fys. Medd. Dan. Vid. Selsk.* 28, No. 8 (1954).
[9] J. Lindhard and M. Scharff, *Phys. Rev.* 124, 128 (1961).
[10] J. Lindhard, *Mat. Fys. Medd. Dan. Vid. Selsk.* 34, No. 4 (1965).
[11] O. B. Firsov, *Zh. Eksp. Teor. Fiz.* 32, 1464 [Engl. transl., *Sov. Phys.—JETP* 5, 1192 (1957)] O. B. Firsov, *Zh. Eksp. Teor. Fiz.* 33, 696 [Engl. transl., *Sov. Phys.—JETP* 6, 534 (1958)].
[12] O. B. Firsov, *Zh. Eksp. Teor. Fiz.* 36, 1517 [Engl. transl., *Sov. Phys.—JETP* 9, 1076 (1959)].
[13] J. Lindhard, M. Scharff, and H. E. Schiøtt, *Mat. Fys. Medd. Dan. Vid. Selsk.* 33, No. 14 (1963).

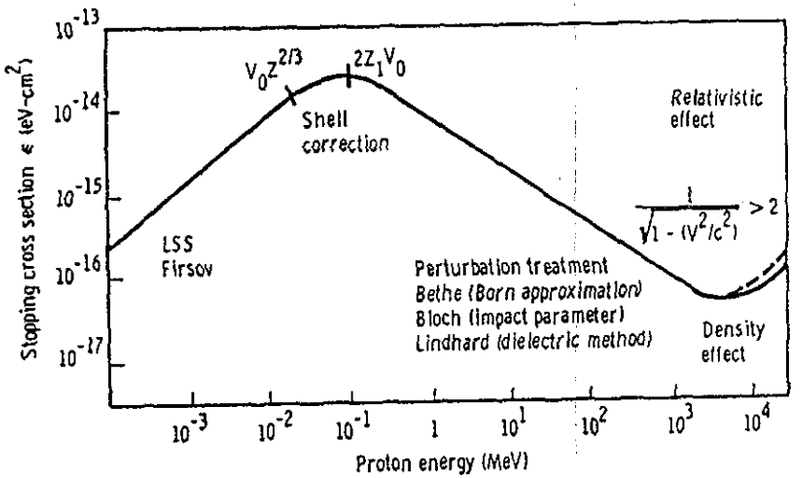

FIG. 1. Stopping cross section of protons in silicon. The general shape is described by various theories for various energy regions.

however, produce different effects in targets. In studying radiation damage, for example, one should focus on the nuclear stopping cross section. This part has a separate chapter on this subject.

For ions heavier than protons, the energy loss behavior is very similar to that of protons. In Fig. 2 we repeat the curve for proton energy loss in

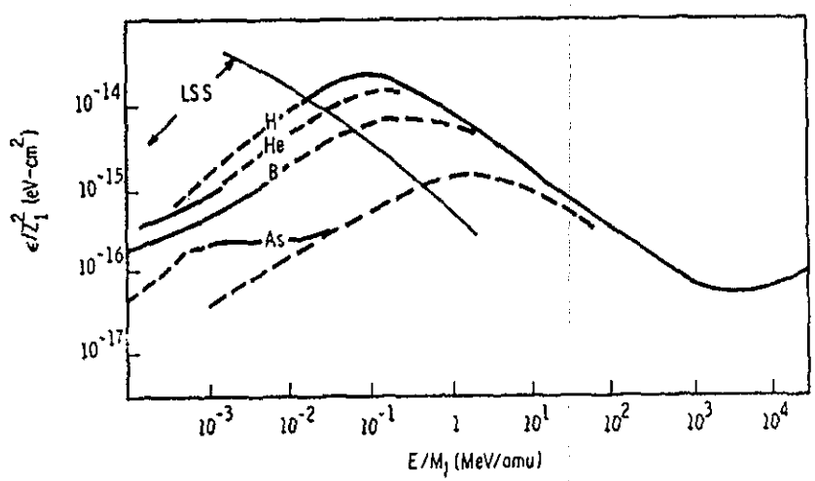

FIG. 2. Family of curves of stopping cross section for heavy ions in silicon. Based on Northcliffe and Schilling's tabulation (1970).[14]

silicon, simply changing the coordinates to ϵ/Z_1^2 for the normalized (or scaled) stopping cross section and to E/M_1 for the velocity parameter. For protons as projectiles, $Z_1 = M_1 = 1$; the curve is the same in Fig. 2 as in Fig. 1. One might object to the use of E/M_1 at relativistic velocities, but that is a minor detail. By presenting Fig. 2 with the normalized parameters, we can see several trends in the stopping cross section as a function of the projectile. The values of stopping cross sections in Figs. 1 and 2 are obtained from Northcliffe and Schilling.[14] The several features one can observe from Fig. 2 are:

(1) At high velocities, ϵ/Z_1^2 tends to converge to a single curve.
(2) For higher Z_1, the position of the peak in ϵ/Z_1^2 occurs at a higher velocity, and its location scales with Z_1.
(3) At lower velocities, the curves in the ϵ/Z_1^2 family are nearly parallel.
(4) At very low velocities, the nuclear stopping cross section begins to influence the curves. The larger the mass number of the projectile, the larger the influence.

These observations are purely empirical and phenomenological. However, various theories for various velocity regions give detailed descriptions of the behavior of stopping cross section as a function of the projectile, its velocity, and the target atoms.

We start our analysis with light ions at high velocities, where many of the ion beam analyses are applied. We then discuss the low-velocity region, where most of the ion implantation work is done and where nuclear stopping plays a role.

2.3. Energy Loss Theories: General Background

In this chapter, we briefly describe various theoretical treatments of energy loss. We keep the discussion at a very elementary level in order to provide the general background needed in extracting information on energy loss. Those interested in detailed theoretical treatments are referred to the excellent review articles by Sigmund.[1] When a charged particle penetrates a material and collides with a target nucleus, the projectile deflects and the target nucleus recoils. This deflection phenomenon is well described by Rutherford's scattering law, which provides an accurate description of large-angle scattering, but these so-called single Coulomb scatterings are very rare events, and are by no means the majority of the projectile scattering events. Most of the projectiles pass nearby multi-

[14] L. C. Northcliffe and R. F. Schilling, *Nucl. Data Tables* 7A, 233 (1970).

tudes of atoms and interact with the circumnuclear electrons as well as with the atomic nucleus. At high velocities, as we shall see, almost all of the energy loss of the projectiles results from projectile–electron encounters, and almost all of the scattering deflection from projectile–nuclear encounters.

The theoretical treatments of inelastic collisions of charged particles with target atoms or molecules deal with fast collisions and/or with slow collisions. The criterion used in making this separation is the velocity of the projectile relative to the mean orbital velocity of the atomic or molecular electrons in the shell or subshell of a given target atom, for which the inelastic process is being considered. When the projectile velocity v is much greater than that of an orbital electron (fast-collision case), the influence of the incident particle on an atom may be regarded as a sudden, small external perturbation. This picture leads to Bohr's theory of stopping power.[3,4] The collision produces a sudden transfer of energy from the projectile to the target electron. The energy loss of a fast particle to a stationary nucleus or electron can be calculated from Rutherford scattering.

2.3.1. Coulomb Scattering and Energy Loss

When a projectile of mass M_1 with atomic number Z_1 at velocity v collides with a target of mass M_2 and atomic number Z_2, the projectile is deflected because of the Coulomb interaction, and the well-defined Kepler motion gives

$$\tan(\theta/2) = b/2p, \tag{2.3.1}$$

where θ is the scattering angle in the center of mass system, p the impact parameter, and b the collision diameter, which is the distance of closest approach on a head-on collision:

$$Z_1 Z_2 e^2/b = \tfrac{1}{2} M_0 v^2. \tag{2.3.2}$$

Here M_0 is the reduced mass of the scattering system:

$$M_0 = M_1 M_2/(M_1 + M_2). \tag{2.3.3}$$

From conservation of energy and momentum, we derive maximum energy transfer to the target particle for a head-on collision as

$$T_{\max} = \frac{4M_1M_2}{(M_1 + M_2)^2} E \tag{2.3.4}$$

and the energy transfer for a general case is

$$T = T_{\max} \sin^2(\theta/2). \tag{2.3.5}$$

With Eqs. (2.3.1) and (2.3.5) the energy transfer becomes

$$T = \frac{T_{max}}{1 + (2p/b)^2}. \tag{2.3.6}$$

The differential scattering cross section can be written as

$$d\sigma = 2\pi p\, dp. \tag{2.3.7}$$

Substituting Eqs. (2.3.6) and (2.3.7) into Eq. (2.2.4), we express the energy lost to the nuclei as

$$S_n = \int T\, d\sigma = T_{max} 2\pi \int_{p_{min}}^{p_{max}} \frac{p\, dp}{1 + (2p/b)^2}. \tag{2.3.8}$$

From Eq. (2.3.6), this equation can be written as

$$S_n = T_{max}(b/2)^2 \pi \int_{T_{min}}^{T_{max}} dT/T \tag{2.3.9}$$

and therefore

$$S_n = \frac{2\pi Z_1^2 Z_2^2 e^4}{M_2 v^2} \ln \frac{T_{max}}{T_{min}} \tag{2.3.10}$$

The low-energy limit T_{min}, which corresponds to p_{max}, has been arbitrarily introduced to avoid divergence in the integration. At a very great distance, the nuclei are shielded by the electrons, and the interaction potential between the projectiles and the target nuclei is no longer $1/r^2$. For the interaction between the projectile and target electrons, no energy whatever will be transferred, if this energy is less than the ionization or excitation of the electron.

When the derivation is repeated for the electrons, the mass of the target electron becomes m rather than M_2 and the charge of the electron is 1 rather than Z_2; Eq. (2.3.10) then gives

$$S_e(\text{per electron}) = \frac{2\pi Z_1^2 e^4}{m v^2} \ln \frac{T_{max}}{T_{min}}. \tag{2.3.11}$$

Because there are Z_2 electrons per target atom, the electronic energy loss per atom will be Z_2 times Eq. (2.3.11):

$$S_e = \frac{2\pi Z_1^2 Z_2 e^4}{m v^2} \ln \frac{T_{max}}{T_{min}}. \tag{2.3.12}$$

The nuclear energy loss is much less than the electronic energy loss, because the ratio of Eq. (2.3.12) to Eq. (2.3.10) gives

$$\frac{S_n}{S_e} = \frac{Z_2 m}{M_2} \simeq \frac{1}{2} \frac{\text{mass of electron}}{\text{mass of proton}} \simeq \frac{1}{4000}. \tag{2.3.13}$$

Equation (2.3.12) can be derived in many different ways. One necessary condition is that the projectiles must be moving much faster than the target electrons, which therefore can be treated as stationary. When the projectile velocity is compared with that of the most loosely bound target electrons, we get

$$v \gg v_0 = \frac{e^2}{\hbar} = \frac{c}{137}. \tag{2.3.14}$$

In the opposite case, if the projectiles are slow enough, all the electrons can adjust their orbital motion in accordance with the instantaneous positions of the projectiles, and therefore are expected to absorb comparatively little energy from them during a scattering event. Hence less electronic energy is lost at low energies (Figs. 1 and 2). This is a part of the adiabaticity argument of Bohr.[3] Other considerations—collision time, electron revolutional frequencies, and so on—complicate the matter further.

Rutherford scattering can provide only a crude estimate of electronic energy loss. It is not a sufficient basis for electron-stopping theories, whose evolution is briefly outlined in the next section.

2.3.2. Perturbation Method and Dielectric Description

A very good approximation is made for the case in which projectiles do not pass close to the target nucleus. One can assume that the direction of motion and the speed of the projectiles are essentially unchanged by the soft collision, and that neither the atomic nucleus nor its surrounding electrons move appreciably while the projectile is traversing the target atom. The momentum transferred from the projectile to the electron is perpendicular to the momentum of the projectile. From this transfer one can calculate the energy lost from the projectile to the target electrons; the result of such calculations leads to a formula similar to Eq. (2.3.12).

The energy loss problem can also be approached from a dielectric description that was suggested by Fermi[15] and developed by Kramers[16] and Lindhard.[10] The description starts with a point charge moving with a constant velocity, producing an electric field. The force F acting on the projectile when it is traversing a medium is dE/dx and is given by

$$\mathbf{F} = Z_1 e(\mathbf{E}_{medium} - \mathbf{E}_{vacuum}), \tag{2.3.15}$$

where E is the electric field of the moving point charge.

[15] E. Fermi, *Z. Phys.* 29, 315 (1924).
[16] H. A. Kramers, *Physica* 13, 401 (1947).

Both the perturbation treatment and the dielectric treatment lead to a formula very similar to Bethe's formula discussed in the next section.

2.3.3. Bethe Formula

Most of the classical treatment of energy loss is based on a well-defined physical length, e.g., impact parameter p or collision diameter b ($=2Z_1Z_2e^2/M_0v^2$). When the latter becomes of the order of the de Broglie wavelength λ ($=\hbar/M_0v$), quantum-mechanical treatment is required. Thus the criterion for the validity of the classical treatment is $b \gg \lambda$ or

$$x \equiv b/\lambda = 2Z_1Z_2e^2/\hbar v \gg 1. \tag{2.3.16}$$

When this condition is not fulfilled, Bethe's quantum theory of electronic stopping[5-7] is derived. It is based on a plane-wave Born approximation, which is a quantum-mechanical perturbation calculation. Such a treatment leads to a nonrelativistic stopping formula:

$$S_e = \frac{4\pi Z_1^2 Z_2 e^4}{mv^2} \log \frac{2mv^2}{I}, \tag{2.3.17}$$

where I is the mean ionization and excitation energy, defined by

$$\log I = \sum_n f_n \log(E_n - E_0), \tag{2.3.18}$$

where E_0 is the ground state of the target atom, E_n the excited state, and f_n the strength of the dipole oscillator.

The complete Bethe formula for electronic stopping of high-velocity charged particles is

$$\frac{1}{N}\frac{dE}{dx} = \frac{4\pi Z_1^2 Z_2 e^4}{mv^2} \log \frac{2mv^2}{I} - \left[\log\left(1 - \frac{v^2}{c^2}\right) - \frac{v^2}{c^2} - \frac{C}{Z_2} - \frac{\delta}{2}\right]. \tag{2.3.19}$$

The two terms containing v^2/c^2 are the relativistic correction terms. C/Z_2 is a velocity-dependent term, significant only at low velocities, which is included to correct the stopping cross section for the nonparticipation of inner-shell electrons in ionization and excitation of projectiles at low velocities. The $\delta/2$ term, another correction to stopping cross section, is important only at ultrahigh velocities; it corrects for the density effect, reducing energy loss from the dashed line to the solid line in the high-velocity region of Fig. 2. This subject has been reviewed by Crispin and Fowler.[17] Both C/Z_2 and $\delta/2$ are functions of the target atom as well as the projectile velocity.

[17] A. Crispin and G. N. Fowler, *Rev. Mod. Phys.* 42, 290 (1970).

Bethe's theory gives a very accurate value for the energy lost by fast ojectiles in elemental targets, provided that the input values I and C/Z_2 e accurate. At the high-velocity limit, C/Z_2 becomes less important; e energy-independent parameter I can be extracted from a careful mea- rement of energy loss. Such measurements, as a function of energy at w energies, provide combined information on log I and C/Z_2. That is, iowing I and C/Z_2, one can extract energy loss values by the Bethe for- ula for fast-moving ions with very high accuracy. We briefly discuss I id C/Z_2 next.

3.4. Mean Excitation and Ionization Energy I

In this section we focus our attention on the mean excitation and ioniza- on energy I of Eqs. (2.3.17) and (2.3.19). I gives the stopping property f a given target Z_2, and is some energy that target electrons can obtain om a very fast projectile. This term is a weighted average of all the ex- itation and ionization processes possible for a given atom. For light arget atoms each of which contains very few electrons, this value can be alculated by quantum-mechanical methods. Because of the complexity f this calculation, however, I is typically determined empirically from ery accurate measurements of energy loss or range.

Bloch's relation[18,19] gives an approximation, based on the Thomas–ermi model of atoms, for estimating I for heavy elements. This relation tates

$$I = Z_2 I_0 \qquad (I_0 \simeq 10 \text{ eV}). \tag{2.3.20}$$

Fano[20] and Turner[21] have reviewed both theoretical and experimental determinations of I. Chu and Powers[22,23] made a statistical calculation of I, using Lindhard and Scharff's[9,24] approach with Hartree–Fock–Slater wave functions. Their results, plus some independent calculations for a few elements and some experimental measurements, are given in Fig. 3. Oscillation of I/Z_2 is observed, and the calculated results show excellent agreement with the experimental values, especially for the region studied by Andersen *et al.*,[25] $Z_2 = 20$–30.

[18] F. Bloch, *Ann. Phys.* 16 (5), 287 (1933).
[19] F. Bloch, *Z. Phys.* 81, 363 (1933).
[20] U. Fano, *in* "Studies in Penetration of Charged Particles in Matter," Nat. Acad. Sci.—Nat. Res. Council, Publ. 1133, Washington, D.C., 1964.
[21] J. E. Turner, *in* "Studies in Penetration of Charged Particles in Matter," Nat. Acad. Sci.—Nat. Res. Council, Publ. 1133, Washington, D.C., 1964.
[22] W. K. Chu and D. Powers, *Phys. Lett.* 38A, 267 (1972).
[23] W. K. Chu and D. Powers, *Phys. Lett.* 40A, 23 (1972).
[24] J. Lindhard and M. Scharff, *Mat. Fys. Medd. Dan. Vid. Selsk.* 27, No. 15 (1953).
[25] H. H. Andersen, H. Sørensen, and P. Vajda, *Phys. Rev.* 180, 373 (1969).

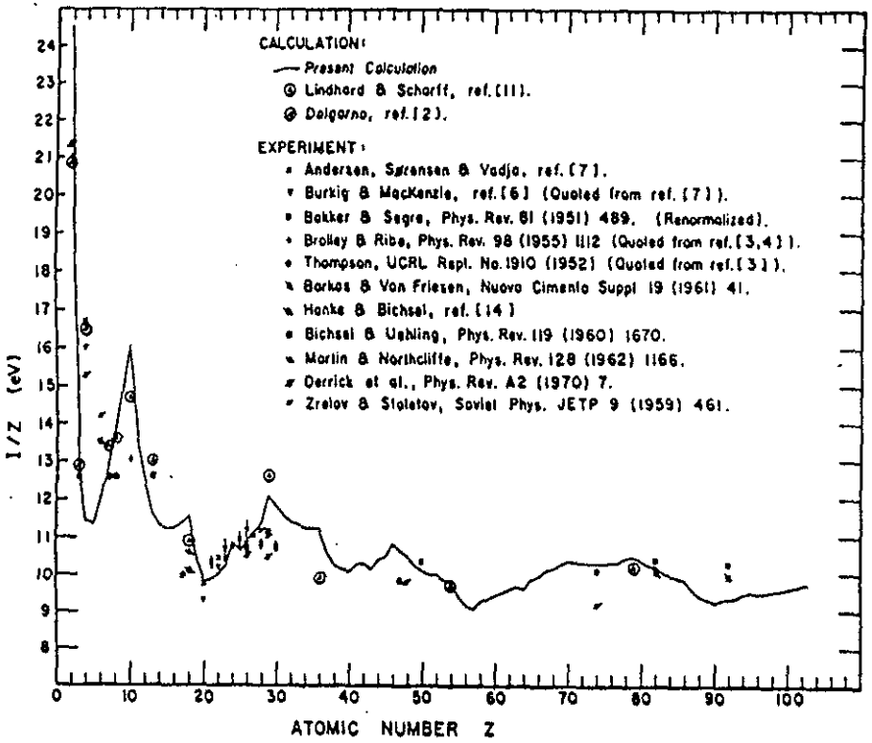

FIG. 3. *Calculation of mean excitation energy by Lindhard and Scharff's theory with a* Hartree–Fock–Slater charge distribution. The calculation I/Z vs. atomic number Z reveals structure, as was observed in many experimental measurements cited in the figure. From Chu and Powers (1972).[23,33]

The results given in Fig. 3 can be used as a guide for normalization and interpolation. For reliable values, I must always be determined empirically.

2.3.5. Shell Correction

Equation (2.3.19) contains a term C/Z_2 to correct for the nonparticipation of inner-shell electrons in the stopping power. When the projectile is extremely fast, all the target electrons contribute to the stopping power more predictably. When the projectile is not so fast, the inner-shell electrons contribute less to the stopping power, and the shell correction term enters in to account for the fact that a single variable I is insufficient to express the stopping problem. Since the correction is due to inner shells,

it can be expressed as

$$C/Z_2 = (C_K + C_L + \cdots)/Z_2, \tag{2.3.21}$$

where C_K and C_L mean corrections to the K shell and the L shell stopping power. Shell corrections have been treated by Walske.[26] Empirically, a careful energy loss measurement should yield C/Z_2 and I. It is easy to see that if one ignores the density effect, a measurement of ϵ vs. E enables one to extract a single energy-dependent parameter X following Bichsel's treatment,[27] where

$$X = \log I + (C/Z_2). \tag{2.3.22}$$

The mean excitation and ionization energy I is independent of energy; the shell correction C/Z_2 is a function of energy, whose value approaches zero at very high energies. In principle, these two boundaries make it possible to separate the two terms. In practice, any small error in experimental measurements will be amplified in the extraction of C/Z_2 and I. Once C/Z_2 and I are determined, values of ϵ vs. E can be obtained for light projectiles in a very broad energy region.

So much for the energy dependence of ϵ in the region of Bethe's formulation. In the next section we discuss the dependence of energy loss on the projectile.

2.3.6. Dependence of Energy Loss on Z_1

The basic result of the Bethe theory is that the energy loss is a property of the target medium and also a function of the projectile velocity. The nature of the projectile enters in only as a scaling factor Z_1^2 in Eqs. (2.3.17) and (2.3.19). Hence stopping power can be extrapolated from one projectile to another by the relation

$$\frac{1}{Z_A^2}\left(\frac{dE}{dx}\right)_{A,v} = \frac{1}{Z_B^2}\left(\frac{dE}{dx}\right)_{B,v}, \tag{2.3.23}$$

where A and B are the atomic numbers of two different projectiles. Both projectiles are moving at a velocity v, which is sufficiently high that they are totally ionized, that is, are bare nuclei without electrons. Because of the Z_1^2 scaling, ϵ/Z_1^2 vs. velocity becomes a unique curve at high velocities—as we can see in Fig. 2, where all the curves merge into the proton-stopping curve. At not too high a velocity, a heavy projectile carries electrons such that the average net charge of the ion is no longer Z_1

[26] M. C. Walske, *Phys. Rev.* 88, 1283 (1952); *ibid.* 101, 940 (1956).

[27] H. Bichsel, *In* "Studies in Penetration of Charged Particles in Matter," Nat. Acad. Sci.—Nat. Res. Council, Publ. 1133, Washington, D.C., 1964.

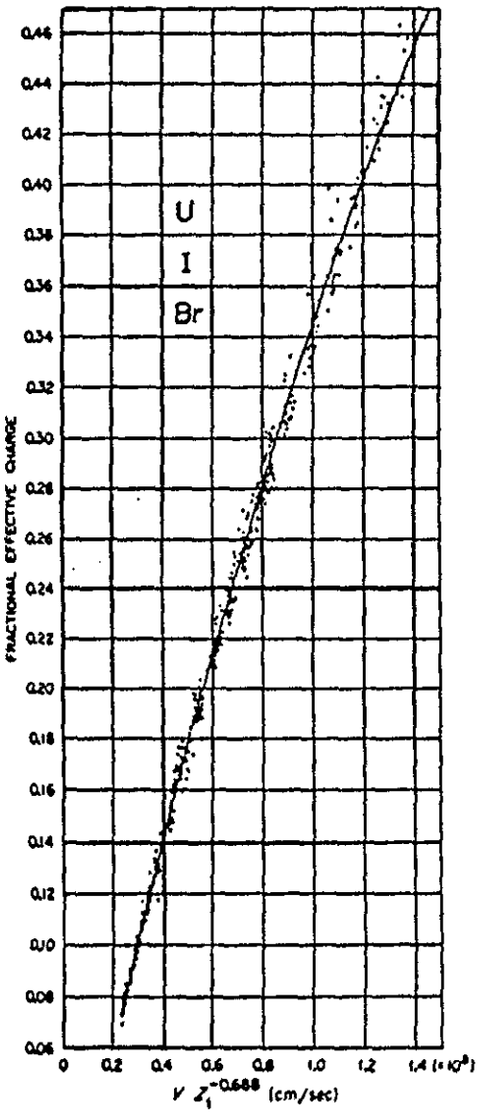

FIG. 4. Measured electronic stopping powers for uranium, iodine, and bromine ions in foils of carbon, aluminum, nickel, silver, and gold, plotted as Z^*/Z_1 vs. $Z_1^{-0.688}$, where Z^* is defined by Eq. (2.3.24), with the proton stopping power taken from Northcliffe and Schilling. The full-drawn line is a least-squares fit to Eq. (2.3.22), with $C = 1.034$ and $p = 0.688$. From Brown and Moak (1972).[38]

but Z_1^*. A generalized scaling that applies to a very broad velocity region becomes

$$\frac{1}{Z_A^{*2}}\left(\frac{dE}{dx}\right)_{A,v} = \frac{1}{Z_B^{*2}}\left(\frac{dE}{dx}\right)_{B,v}, \tag{2.3.24}$$

where Z_A^* and Z_B^* are the effective charges of moving ions A and B traveling at velocity v, which could be considerably below the Bethe velocity region.

This type of scaling from one projectile to another has been demonstrated by Brown and Moak.[38] They measured the stopping powers for uranium, iodine, and bromine ions in foils of carbon, aluminum, nickel, silver, and gold in various velocity regions. They extracted the fractional effective charge Z_1^*/Z_1 from Eq. (2.3.24) by comparing their energy loss measurement to the published values of proton energy loss. This fractional effective charge is then plotted as a function of velocity times $Z_1^{-0.688}$. In their figure, reproduced here as Fig. 4, the solid curve is a least-squares fit to an equation representing Betz's[29] formula:

$$Z_1^*/Z_1 = 1 - C\exp(-v/v_0 Z_1^{\gamma}) \tag{2.3.25}$$

where the fitting parameters $C = 1.034$ and $\gamma = 0.688$ are as obtained by Brown and Moak.[38] Recent measurements by Ward *et al.*[30] confirm the scaling of energy loss as given by Eq. (2.3.24). Ziegler[31] recently modified Eq. (2.3.25) by curve-fitting a large number of ion–target combinations over a wide energy region, and obtained consistent results among the measurements of energy lost by heavy ions.

2.3.7. Low-Velocity Electronic Energy Loss

At low velocities the Bethe formula does not apply to electronic stopping, because the inner-shell electrons contribute less to the stopping power. This reduction gives a very large correction. Also at very low velocities, the neutralization probability becomes so large that the collision between the projectile and the surrounding electrons is almost elastic in a reference frame moving with the ion. The energy loss then becomes proportional to the velocity of the projectile. Lindhard, Scharff, and Schiøtt[13] (abbreviated as LSS) and Firsov[11,12] gave theoretical descriptions for this energy region. The LSS expression is based on elastic scat-

[38] M. D. Brown and C. D. Moak, *Phys. Rev.* B6, 90 (1972).
[29] H. D. Betz, *Rev. Mod. Phys.* 44, 465 (1972).
[30] D. Ward, J. S. Forster, H. R. Andrews, I. V. Mitchell, G. C. Ball, W. G. Davies, and G. J. Costa, unpublished, AECL-5313, Chalk River, Canada (1976).
[31] J. F. Ziegler, *Appl. Phys. Lett.* 31, 544 (1977).

tering of free target electrons in the static field of a screened point charge. Firsov's expression is based on a simple geometric model of momentum exchanged between the projectile and the target atom during interpenetration of electron clouds. Both theories adequately describe the general behavior of the stopping power with regard to the energy dependence and magnitude of the stopping power.

The beauty of Firsov's approach[11,12] is its simplicity. The geometric model of the interaction of two atoms can be modified easily for more complicated atomic structures. Firsov's approach considers the transfer of momentum from projectile electrons to those of the target atom. An imaginary surface s is constructed between the two atoms at the middle or at the position of the minimum potential. As the projectile interpenetrates the target atom, electrons of one atom, upon reaching the surface s, are assumed to transfer a momentum mv to the other atom. The total momentum transfer per unit time is given by assuming an electron flux $\frac{1}{4}nv_e$, where n is the localized electron density and v_e the velocity of the electrons in the atom. The total energy loss in the collision is related to the impact parameter b by

$$T(b) = \tfrac{1}{4}mv \int_{-\infty}^{+\infty} dx \int_s ds\, nv_e, \tag{2.3.26}$$

and the stopping cross section becomes

$$S_e = \frac{1}{N}\frac{dE}{dx} = \int_{b_0}^{\infty} 2\pi b\, db\, T(b). \tag{2.3.27}$$

From here on, it is up to the user to determine what values of n and v_e to use and how to integrate over the plane s, the distance x, and the impact parameter b.

The beauty of the LSS approach is that by extensive use of the Thomas–Fermi model, similarities among different stopping systems can be obtained, and therefore scaling from one system to the other can be done with adequate accuracy. The reduction of energy, distance, and energy loss into a set of universal units, along with the proper treatment of nuclear energy loss and range study, has made the LSS theory one of the most influential theories on low-energy ion implantation. Because of the complexity of the problem and some necessary but crude approximations in the treatment, deviation between the theoretical calculations and the experimental measurements should not be taken as a surprise.

With respect to electronic energy loss, the major contribution to the difference between theoretical trend and experimental measurements is the charge distribution of a target atom. The smooth distribution described by the Thomas–Fermi model has great significance in producing the general trend of the interaction of charged particles, and allows smooth scaling from one system to another. The Thomas–Fermi statistical treatment of LSS makes it possible to generalize the problems and reduce the parameters in order to form an overall picture of the stopping problem, whereas a Hartree–Fock–Slater charge distribution is very specific and irregular and causes stopping to fluctuate about the norm (LSS). Realizing the difference between the Thomas–Fermi and Hartree–Fock–Slater charge distributions enables one to adjust energy loss theory when necessary.

By the LSS theory, the electronic energy loss at low velocities can be written as

$$S_e = \frac{1}{N}\frac{dE}{dx} = \eta \frac{8\pi e^2 a_0}{N}\frac{Z_1 Z_2}{Z}\frac{v}{v_0} \tag{2.3.28}$$

where $\eta \simeq Z_1^{1/6}$. This relation is thought to be applicable to $v < v_0 Z^{2/3}$.

The energy and depth, in LSS dimensionless units, are

$$\epsilon = E\frac{aM_2}{Z_1 Z_2 e^2 (M_1 + M_2)}, \tag{2.3.29}$$

$$\rho = xNM_2 4\pi a^2 \frac{M_1}{(M_1 + M_2)^2}, \tag{2.3.30}$$

where

$$a = 0.8853 a_0 Z^{-(1/3)} \tag{2.3.31}$$

$$Z = (Z_1^{2/3} + Z_2^{2/3})^{3/2}. \tag{2.3.32}$$

In dimensionless units, the electronic stopping cross section can be expressed as

$$(d\epsilon/d\rho)_e = k\epsilon^{1/2}, \tag{2.3.33}$$

where k is a constant depending on Z_1, Z_2, M_1, and M_2:

$$k = \frac{0.0793 Z_1^{2/3} Z_2^{1/2} (M_1 + M_2)^{3/2}}{Z^{1/2} M_1^{3/2} M_2^{1/2}}. \tag{2.3.34}$$

The values of k are from 0.1 to 0.2 unless the projectile is much lighter than the target atom. E/ϵ, x/ρ, and k for several systems are given in Table I.

2.3.8. Nuclear Energy Loss

Nuclear stopping is a relatively small effect in the Rutherford collision region, as was stated in Section 2.3.1. Its contribution to the total stopping cross section is significant only at low velocities. However, its sig-

TABLE I. LSS Conversion Factors

Target	Ion	E/ϵ (keV)	x/ρ (Å)	k
Si	H	1.163	1480	2.08
	He	2.674	492	0.45
	B	8.850	313	0.24
	As	209	590	0.12
	Sb	515	928	0.11
Ge	H	3.32	6730	5.47
	As	298	668	0.16
	Sb	656	835	0.14
Au	H	10.75	23540	15.1
	As	592	883	0.46
	Sb	1136	837	0.22

nificance in the theory of radiation effects, such as radiation damage, sputtering, and the relation between projected range and total range, makes the study of nuclear collision important. Scattering cross sections for heavy projectiles in the Thomas–Fermi and excessive-screening regions have been reviewed by Sigmund.[32–35]

By the Thomas–Fermi atomic model, the differential cross section can be written as

$$d\sigma = \pi a^2 \frac{dt^{1/2}}{t} f(t^{1/2}), \tag{2.3.35}$$

where t is a reduced variable that contains both dimensionless energy ϵ and the scattering angle θ, that is,

$$t^{1/2} = \epsilon \sin(\theta/2). \tag{2.3.36}$$

This type of cross section leads to a nuclear stopping cross section having the form

$$(d\epsilon/d\rho)_n = f(\epsilon), \tag{2.3.37}$$

which is given in Fig. 5. Electronic stopping cross sections with various values of k are also given in this schematic. From Table I and Fig. 5, one can easily estimate at what energy region the nuclear stopping is comparable to the electronic stopping. For example, for protons bombarding silicon, $k = 2.08$ and electronic stopping dominates the total energy loss, even down to the energy region below 1 keV. For heavy-ion implantation, nuclear stopping dominates in a very large energy region. For example, in arsenic stopping in silicon, Fig. 2 shows the nuclear stopping contribution at low energies.

It should be noted that the same symbol ϵ has been used in two different meanings. One is the LSS unitless energy, defined in Eq. (2.3.29) and

[32] P. Sigmund, *Rev. Roum. Phys.* 17, 823 (1972).
[33] P. Sigmund, *Rev. Roum. Phys.* 17, 969 (1972).
[34] P. Sigmund, *Rev. Roum. Phys.* 17, 1079 (1972).
[35] P. Sigmund, *In* "Physics of Ionized Gases" (M. Kurepa, ed.), p. 137. Inst. Phys., Belgrade, 1972.

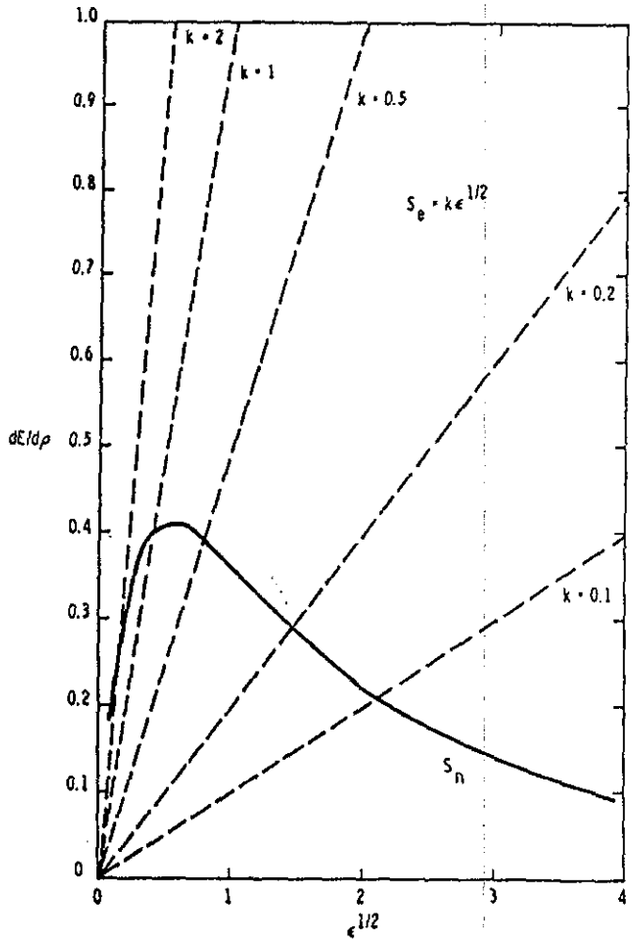

FIG. 5. Nuclear stopping (solid curve) and electronic stopping (dashed curves) as calculated by the LSS theory for various values of k. Light ions in a solid have a large k; heavy ions in a solid have k around 0.1.

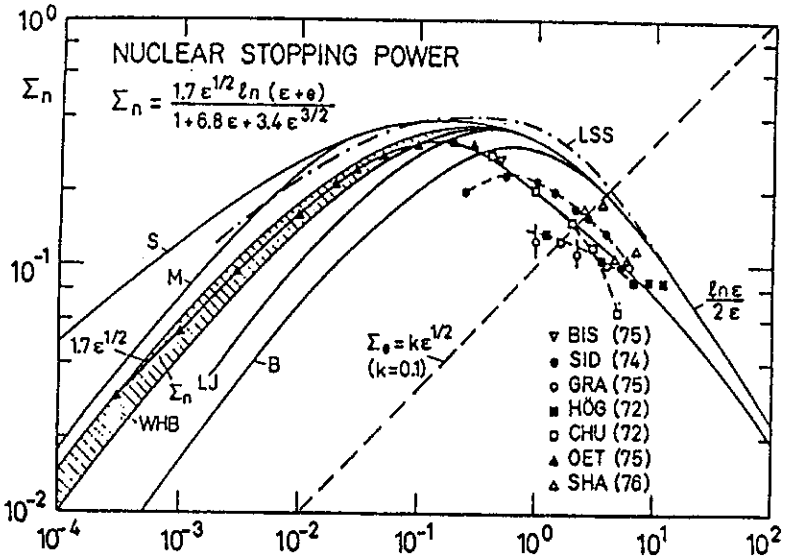

FIG. 6. Nuclear stopping power as a function of energy in LSS units. The points are experimental data; the theoretical curves are based on various potential calculations: S, Sommerfeld; M, Molière; LJ, Lenz–Jansen; B, Bohr; and LSS as in text. For details see Kalbitzer *et al.* (1976).[37]

used throughout the theory in the low-energy region. The other is the stopping cross section, defined by Eq. (2.2.3). Wilson *et al.*[36] and Kalbitzer *et al.*[37] have given a simple universal formula to fit the published data on nuclear stopping power. The version of Kalbitzer *et al.*[37] is

$$\left(\frac{d\epsilon}{d\rho}\right)_n = \frac{1.7\epsilon^{1/2}\ln(\epsilon + e)}{1 + 6.8\epsilon + 3.4\epsilon^{3/2}}, \tag{2.3.38}$$

where here e refers to the natural base 2.718. This formula applies in the range $10^{-4} \leq \epsilon \leq 10^2$, and gives a value much lower than that obtained by the LSS theory.

The nuclear stopping study by Kalbitzer *et al.*[37] is summarized in Fig. 6. In their figure, nuclear stopping power $d\epsilon/d\rho$ is given as a function of energy ϵ, in LSS units. The points denote experimental data quoted in their paper. The curves are theoretical values of nuclear stopping power for various potentials (see the paper by Kalbitzer *et al.*[37] for references). The dashed line represents the electronic stopping power of Eq. (2.3.33) with $k = 0.1$. The solid curve fitted to the experimental points is that of Eq. (2.3.38), which is in good agreement with the calculation by Wilson, Haggmark, and Biersack[36] (WHB curve in Fig. 6).

[36] W. D. Wilson, L. G. Haggmark, and J. P. Biersack, *Phys. Rev. B* 15, 2458 (1977).
[37] S. Kalbitzer, H. Oetzman, H. Grahmann, and A. Feuerstein, *Z. Phys.* A278, 223 (1976).

2.3.9. Electronic Energy Loss in the Medium-Velocity Region

The Bethe formula applies to the high-velocity region (Section 2.3.3), and the LSS and Firsov theories apply to the low-velocity region. For the medium-velocity region, which is the neighborhood of maximum energy loss, there is no adequate theory. The Bethe theory does not work because the charge of the projectile is partly neutralized and because the inner-shell electrons participate less in the stopping power. Accurate knowledge of shell corrections for the target atoms may push the applicability of the Bethe formula into the medium-velocity region, but when $2mv^2 \simeq I$, the value of Eq. (2.3.19) depends entirely on the value of $-C/Z_2$, and the Bethe formula no longer applies in this region. Accurate knowledge of energy loss in this region at the present time can be extracted only by semiempirical methods—which, of course, are also useful in other regions.

For the medium-velocity region, the electronic energy loss can be interpolated by the scaling, as follows:

(1) The scaling of energy loss from the charge state of the projectile (Section 2.3.6) is one of the methods that makes it possible to scale from one projectile to another for a given target at a given velocity.

(2) The three-parameter curve fit by Brice[38] enables one to interpolate an energy loss value from one energy region to another for a given projectile–target combination.

(3) For a given projectile at a given velocity, the energy loss from one target to another can be scaled from a semi-empirical relation that can be calculated by use of the Hartree–Fock–Slater charge distribution. Such a practice has been demonstrated by Ziegler and Chu.[39] As an example, Fig. 7 shows 2-MeV ^{4}He stopping cross section vs. Z_2. The dashed curve was calculated theoretically by the method of Lindhard and Winther,[40] here modified by the use of the Hartree–Fock–Slater atomic wave function. The calculation is similar to that made by Rousseau *et al.*[41] The interpolation suggested by Ziegler and Chu[39] is represented by the solid curve.

The accuracy of the interpolation and extrapolation depends on the amount and the accuracy of the data base used for interpolation. Each case will be different. In general, an accuracy of ± 10% can be reached

[38] D. K. Brice, *Phys. Rev. A* 6, 1791 (1972).
[39] J. F. Ziegler and W. K. Chu, *At. Data Nucl. Data Tables* 13, 463 (1974).
[40] J. Lindhard and A. Winther, *Mat. Fys. Medd. Dan. Vid. Selsk.* 34, No. 4 (1964).
[41] C. C. Rousseau, W. K. Chu, and D. Powers, *Phys. Rev. A* 4, 1066 (1971).

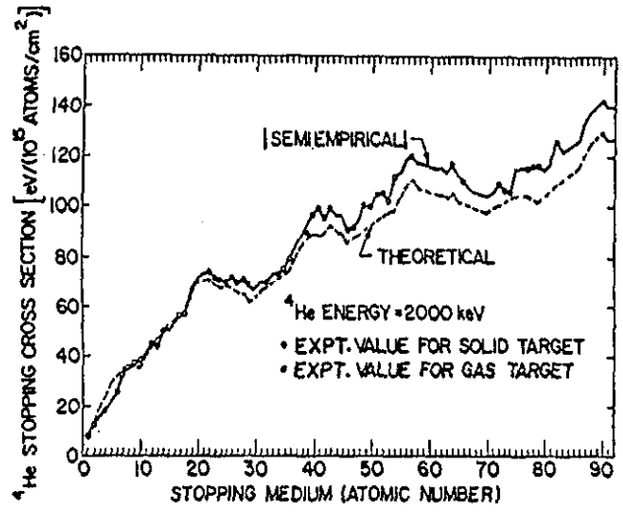

FIG. 7. Semiempirical values of the stopping cross section for a 2000 keV beam of ^{4}He. Also shown are the experimental values on which they are based as well as the theoretical values that were used in interpolation. From Ziegler and Chu (1974).[39]

by proper interpolation. Examples of the method of interpolation can be found in Northcliffe and Schilling,[16] Brown and Moak,[28] Ziegler and Chu,[39] Ward *et al.*,[30] Andersen and Ziegler,[42] and Ziegler.[43]

2.4. Experimental Methods on Energy Loss

Accurate values of energy loss always come from careful measurements. In this section we briefly discuss various experimental methods of measuring energy loss. Some of the methods are very accurate and straightforward and require very little description. Others, especially some of those recently developed, display some novelty. In all cases only one or two representative examples are given to illustrate the method.

There are several different methods of measuring energy loss. One is to prepare a thin foil or thin film, measure the film thickness, and measure the total energy loss of a beam transmitted through the film, to obtain the stopping cross section. Another is to make an indirect measurement of a physical quantity that is related to the stopping cross section in a predictable way, e.g., range, backscattering yield, or Doppler shift of γ emission of compound nuclei in a target medium. All of these are related to energy loss, and therefore an accurate measurement of any one of them will yield information on energy loss. In energy loss measurements, a probable error of 2–4% is typical. A few experimenters have achieved probable error less than 1%.

[42] H. H. Andersen and J. F. Ziegler, "Hydrogen Stopping Powers and Ranges in All Elements," Pergamon Press, New York (1977).

[43] J. F. Ziegler, "Helium: Stopping Powers and Ranges in All Elemental Matter," Pergamon Press, New York (1977).

2.4.1. Transmission Measurements on Thin Foils

The principle of this measurement is to prepare a uniform, self-supported thin foil of the target material and carefully measure the energy of the beam with and without transmission through the foil, to determine the amount of energy loss in the foil.

A thin foil is usually prepared by vacuum-evaporating the target material onto a plastic substrate, which is subsequently dissolved; an example of this method is given by Valenzuela and Eckardt.[44] Foils of some elements can be obtained commercially. The thickness of the foil is usually determined by measuring the mass of the foil on a microbalance or a quartz oscillator during the evaporation and measuring the area of the foil. The mass per unit area is equivalent to the density times the thickness of the foil. It can also be obtained by calibrating the observed energy loss against a given projectile whose stopping cross section in this element is known. Target mass per unit area can be expressed as $\rho\,\Delta s$ or $N\,\Delta x$, to an accuracy ranging from $\pm 0.1\%$ for thick foils to $\pm 2\%$ for thin foils. Thick foils, of the order of 1–10 mg/cm^2, are suitable for protons with high energy (Bethe region), but are too thick for heavy projectiles, especially at medium or low energies. Foils on the order of fractions of 1 mg/cm^2 (e.g., 5–500 μg/cm^2) are difficult to prepare but can also be made by vacuum evaporation.

The energy of the projectile can be measured by any of various instruments: solid-state detectors, electrostatic and magnetic analyzers, and so on. The various methods give measurements with various probable errors. Typically, a transmission experiment gives an accuracy of 2–5%. A few experiments give better accuracy.

As an example, Fig. 8 shows the experimental setup used by Ishiwari *et al.*[45] to measure the energy loss of 7.2-MeV protons in thin foils. The gold foil at the center of the chamber is not the sample; the elastically scattered beam from the gold foil is used in order to avoid damaging the silicon detector as an intense direct beam would do. Targets of alumi-

[44] A. Valenzuela and J. C. Eckardt, *Rev. Sci. Instrum.* 42, 127 (1971).

[45] R. Ishiwari, N. Shiomi, S. Shirai, and Y. Uemura, *Bull. Inst. Chem. Res., Kyoto Univ.* 52, 19 (1974).

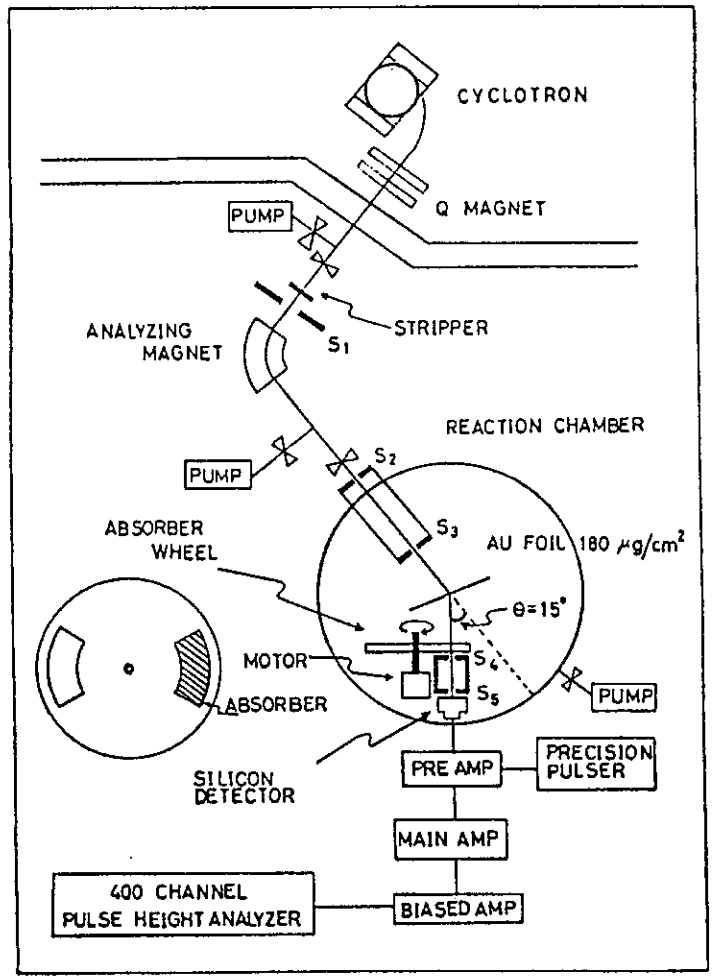

FIG. 8. Experimental setup for the energy loss measurement by the foil transmission method. From Ishiwari *et al.* (1974).[45]

num, titanium, iron, copper, molybdenum, silver, tin, tantalum, and gold foils, 10–20 mg/cm² thick, are mounted on the absorber wheel at lower left. This experimental setup is typical for transmission measurements of energy loss. Ishiwari's measurements are accurate to within ±0.3–0.5%.

Another very accurate method for measuring energy loss was developed by Andersen *et al.*[46] By this method, called the calorimetric

[46] H. H. Andersen, A. F. Garfinkel, C. C. Hanke and H. Sørensen, *Mat. Fys. Medd. Dan. Vid. Selsk.* 35, No. 4 (1966).

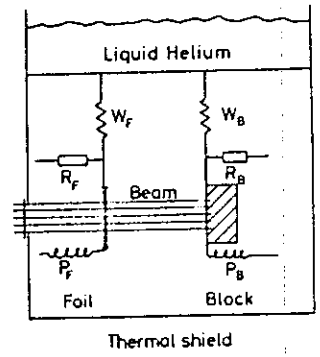

FIG. 9. Stopping power measuring system. W_F and W_B are thermal resistances, R_F and R_B thermometers, and P_F and P_B electrical heaters. From Andersen *et al.* (1966).[46]

method, the amount of heat that the projectiles give to the foil is measured. The principle of this method is illustrated in Fig. 9. A target foil of good heat conductivity is connected to a thermal resistance W_F, a thermometer R_F, and a heating coil P_F. Behind the target foil, a block of gold or any heat-conducting material whose thickness is greater than the range of the transmitted beam is connected to a thermal resistance W_B, a thermometer R_B, and a heating coil P_B. The measuring equipment is fastened to the bottom of a liquid-helium cryostat. The thermometer is an ordinary 0.1 W carbon resistor. The change in resistivity gives accurate temperature measurement at low temperatures.

The proton beam at energy E_0, as it passes through the foil and is stopped in the block, will cause a heating of the foil and block, raising the temperature of both as measured by R_F and R_B thermometers. The beam is then switched off, and electrical powers P_F and P_B are fed to heaters thermally connected to the foil and block, to produce the same temperature rise. The power is proportional to the amount of energy deposited in the foil and in the block; therefore the energy deposited in the foil is ΔE and will be related to the incident energy E_0 by

$$\Delta E/P_F = E_0/(P_F + P_B). \tag{2.4.1}$$

The energy loss of 5–12-MeV protons and deuterons in various metals can be measured by this method with an accuracy of ±0.4%.

The above two examples (Figs. 8 and 9) represent two sets of the most accurate measurements of energy loss. Both types of experiments are reported with a probable error of less than 0.5%. However, the measurements by Ishiwari *et al.* are consistently 1.7–3.4% lower than those by Andersen *et al.* (Fig. 9). The difference is small, but outside the probable errors quoted.

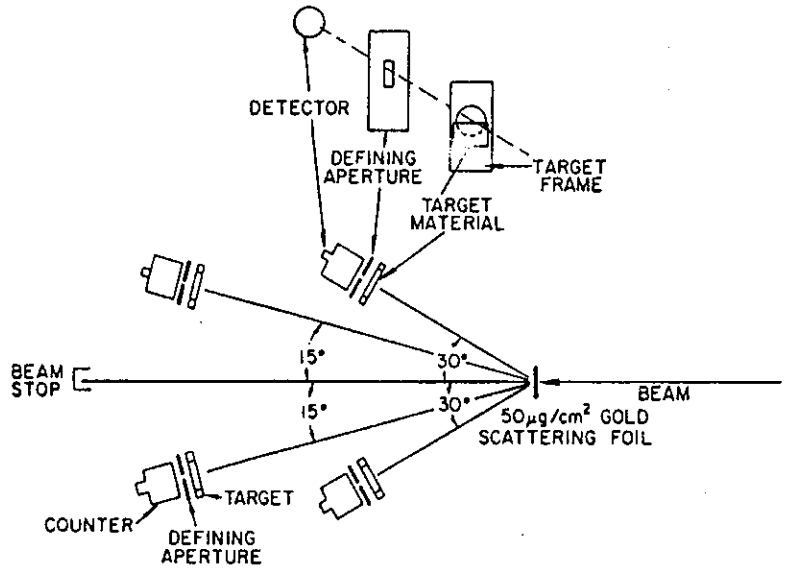

FIG. 10. The experimental arrangement for measuring ΔE. The gold scattering foil acts as a low intensity source of ions for the four target–counter arrays. This permits the measurement of ΔE values for four target materials simultaneously. As can be seen in the exploded view, each target frame is only half covered with the target material. Thus only half of the ions that reach the counter have suffered energy loss. From Ward *et al.* (1972).[47]

The energy loss of heavy ions can be measured by transmission only when the projectiles have enough energy to go through a self-supported foil. As an example, Ward *et al.*[47] have measured energy losses of approximately 1–3.5-MeV/amu ions transmitted through various metallic foils. Their experimental setup is given in Fig. 10. A high-energy ion beam from a tandem accelerator passes through a thin gold foil, which acts as a low-intensity source of ions for four to six target–counter arrays. Thus ΔE values for several target materials can be measured simultaneously. As can be seen from the enlarged view of the target setup in Fig. 10, each target frame is only half-covered with target foil; thus only half of the ions suffer energy loss. With this target arrangement, energies of projectiles can be measured with and without energy loss due to passing the foil. Some of the energy spectra are given in Fig. 11. The incident energies are calculated from the known scattering angles. The shift of the peak gives a measurement of ΔE, and independent measurement of $\rho\ \Delta x$ gives $dE/\rho\ dx$. An overall uncertainty of about 4% is claimed for these measurements.

[47] D. Ward, R. L. Graham, and J. S. Geiger, *Can. J. Phys.* 50, 2302 (1972).

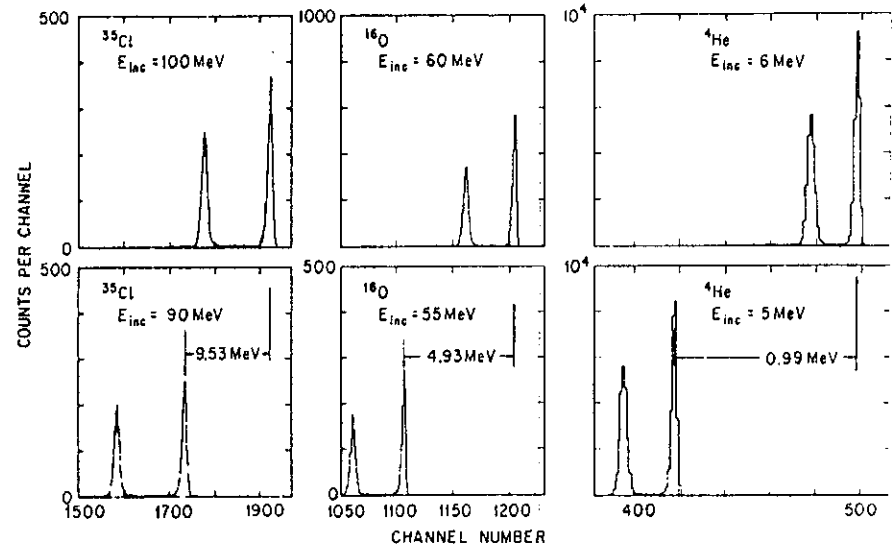

FIG. 11. Some of the spectra obtained with the apparatus shown in those ions which have lost energy in traversing the target material. The energy of the higher peak is calculated from the known incident beam energy E_{inc} and the accurately known scattering angle (15° or 30°). The shifts of the upper peak position with incident-beam energy provide the energy calibration of the counting system. From Ward *et al.* (1972).[47]

High-precision transmission measurements can be made only when the foil is thick enough. For foils a fraction of 1 mg/cm² thick, the uncertainty in the foil thickness will be greater than ±1–2%. A recent measurement of energy loss and energy straggling of protons and helium ions in the energy region 20–260 keV on thin metal foils by Eckardt[48] has a probable error of 2–7%.

2.4.2. Transmission Measurements on Gaseous Targets

There are many measurements of energy loss of protons and α particles in gaseous targets. Typically a gaseous target is contained in a differentially pumped gas cell or a gas cell with thin windows. The thickness of the gas target $N\ \Delta x$ is related to the physical length of the gas cell Δx and the number of gas particles per unit volume N; by the ideal gas law,

$$N = 9.565 \times 10^{15}(P/T), \qquad (2.4.2$$

where P is the pressure of the gas (Torr), and T the temperature of the gas (°K).

[48] J. C. Eckardt, unpublished (1976).

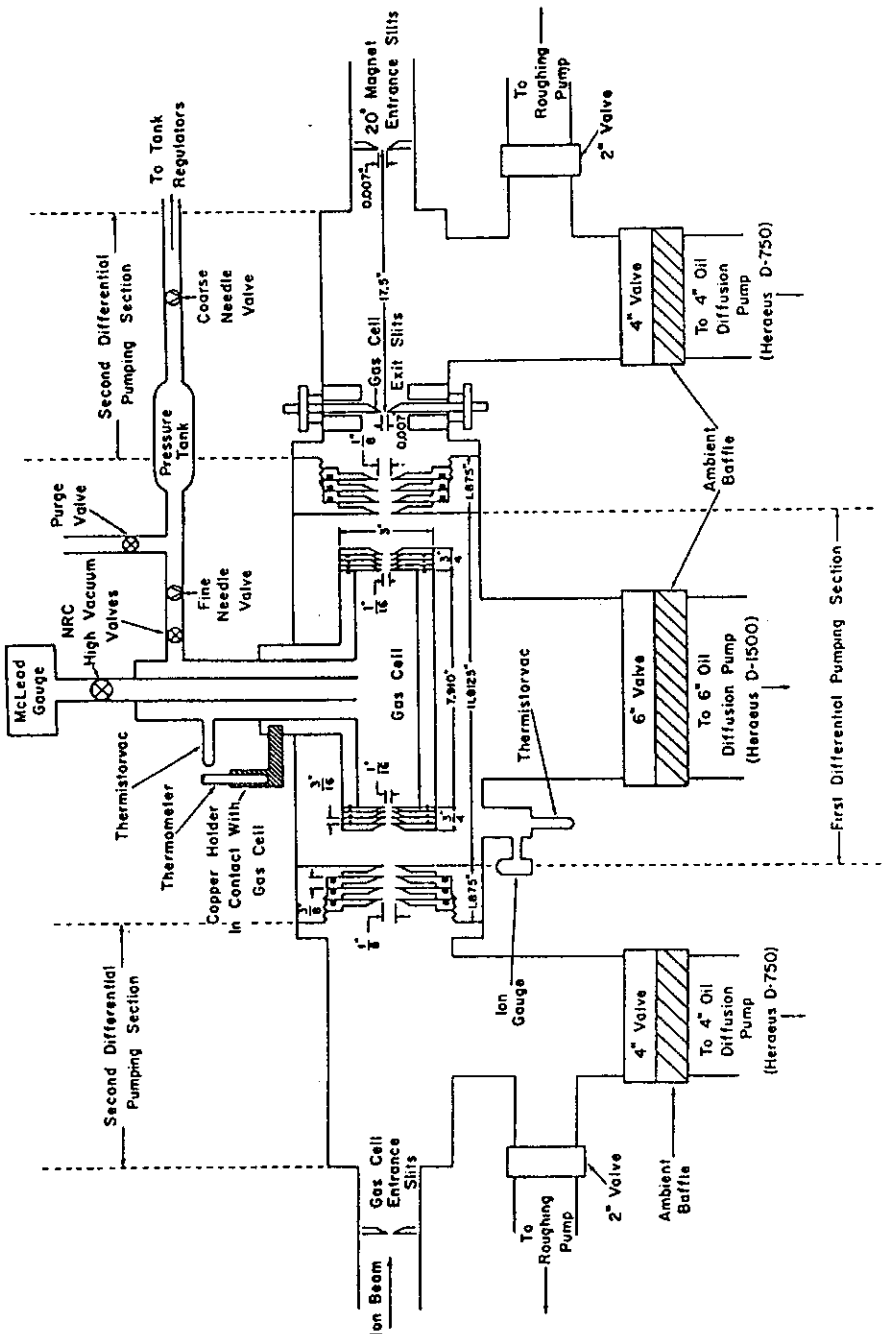

FIG. 12. A differential pumping gas cell system. From Bourland *et al.* (1971).[49]

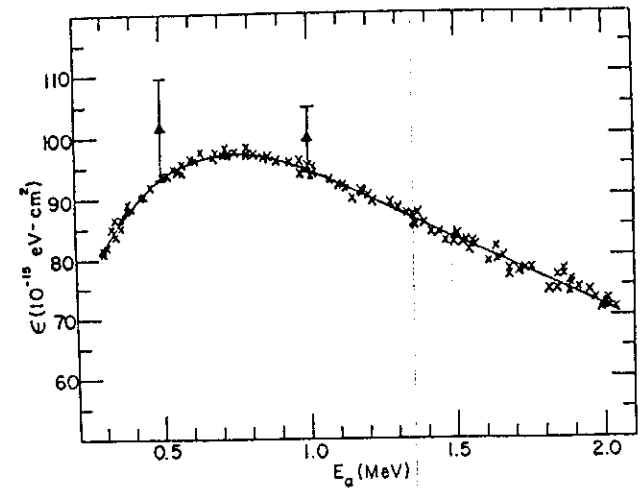

FIG. 13. Stopping cross section of α particle in oxygen gas. The smooth curve is an average-value curve drawn through the measurements, and the triangles are measurements by Rotondi. From Bourland *et al.* (1971).[49]

A typical experimental setup for the differentially pumped gas cell is given in Fig. 12. This example is extracted from Bourland *et al.*[49] Their gas cell has two-stage pumping and is 21.5 cm long. An end correction to this length for the pressure in the differential pumping section is less than 2.5%, except that for hydrogen gas the correction is 5%. A typical energy profile for measuring the energy loss of α particles in oxygen is given in Fig. 13. Each energy loss spectrum is made by use of a 60° magnetic spectrometer. A series of measurements at various gas pressures and various incident energies will produce an ϵ vs. E relation. In this experiment, many measurements produce a curve of ϵ vs. E that has a probable error of ± 1–2%. Many other elemental and compound gases are used in this setup (Fig. 12), in the study of the additivity rule for α-particle energy loss in gaseous compounds.

2.4.3. Transmission Measurements on Supported Films

Usually when a film is evaporated onto a substrate, the ion beam can be transmitted through the film but not through the substrate. The consequent difficulty in measuring transmission energy loss can be overcome by using a sharp nuclear resonance. For example, Leminen and Anttila[50] used the ^{27}Al (p, γ) reaction at various resonance energies to measure the

[49] P. D. Bourland, W. K. Chu, and D. Powers, *Phys. Rev. B* **3**, 3625 (1971).
[50] E. Leminen and A. Anttila, *Ann. Acad. Sci. Fenn., Ser. A6*, 370 (1971).

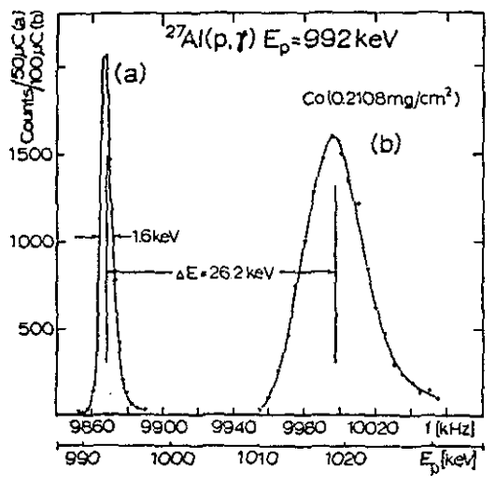

FIG. 14. Gamma yield from the ^{27}Al (p, γ) reaction at E_p = 991.8 keV, *with and without* stopping cobalt layer (0.211 mg/cm²). The thickness of the reacting aluminum is 4 mg/cm². From Leminen and Anttila (1971).[50]

energy loss and energy straggling of 0.6–2-MeV protons in iron, cobalt, and antimony. A very thin aluminum layer, 4 μg/cm², was evaporated onto a tantalum backing. Figure 14 is an example from Leminen and Anttila.[50] Gamma yield from the ^{27}Al (p, γ) reaction at E_p = 991.8 keV is measured as a function of E_p, with and without a stopping cobalt layer. The reacting aluminum layer is 4 μg/cm² thick, the cobalt layer 211 μg/cm². The energy loss of the protons in the absorbing layer is determined by measuring the shift in the centroids of the γ-yield curve. The broadening of that curve gives the energy straggling.

This is a very useful method, but it is very specific. It works only for a projectile in an energy region in which known resonances exist. It is good for measuring the energy loss of protons when the (p, γ) reaction can be used over a broad energy region on several markers. It is not suitable for measuring the energy loss of helium ions or heavy ions at low energies, where no resonance or no sharp γ resonance exists.

2.4.4. Transmission Measurements on a Thin Layer on a Solid-State Detector

The scheme for measuring energy loss of a thin layer in front of a detector is very similar to that diagramed in Fig. 8, where a self-supported foil is placed in front of a solid-state detector. It differs in that since a

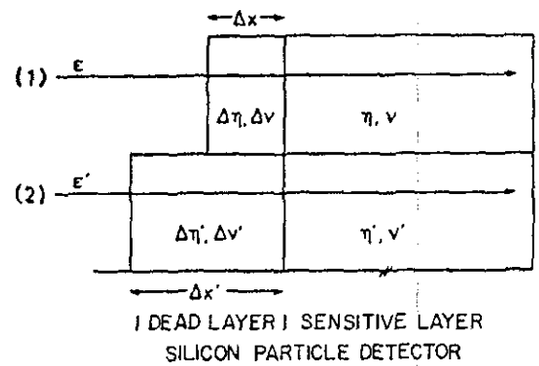

FIG. 15. Schematic for determining electronic (η, Δη) and nuclear (ν, Δν) stopping cross sections. From Grahmann and Kalbitzer (1976).[51]

layer on the detector can be made very thin (a few hundred angstroms), this method can be used for heavy ions at very low energies. These ions can penetrate a very thin film or dead layer on a detector. At very low energies the pulse height of a silicon detector corresponds not to the total energy of a particle that enters the detector, but rather to the electronic energies.

Grahmann and Kalbitzer[51] have used this fact in developing a simple but novel method by which electronic energy loss and total energy loss can be measured directly at very low energies (<60 keV). They use a silicon particle detector with a thin absorbing layer. Different effective thicknesses of this layer can be obtained by tilting the detector with respect to the incident particle beam. In Grahmann and Kalbitzer's experiment, the absorbing layer happens to be a dead layer of 400-Å silicon produced by ion implantation onto a silicon detector. The principle of the method is given schematically in Fig. 15, where the thickness of the dead layer is Δx for one case and $\Delta x'$ for another case, with the detector tilted. For all practical purposes the sensitive layer of the detector is infinitely thick. The total stopping cross section has two components, related by

$$\epsilon = \eta + \Delta\eta + \Delta\nu + \nu \qquad \text{for} \quad \Delta x \text{ layer}, \tag{2.4.3}$$

where ϵ is ion energy, $\Delta\eta$ and $\Delta\nu$ electronic and nuclear energy losses in the absorbing layer Δx, and ν the nuclear energy loss in the sensitive layer. The total ionization yield η is measurable and is the response of the solid-state detector. By tilting or evaporating to increase the effec-

[51] H. Grahmann and S. Kalbitzer, *Nucl. Instrum. Methods* 132, 119 (1976).

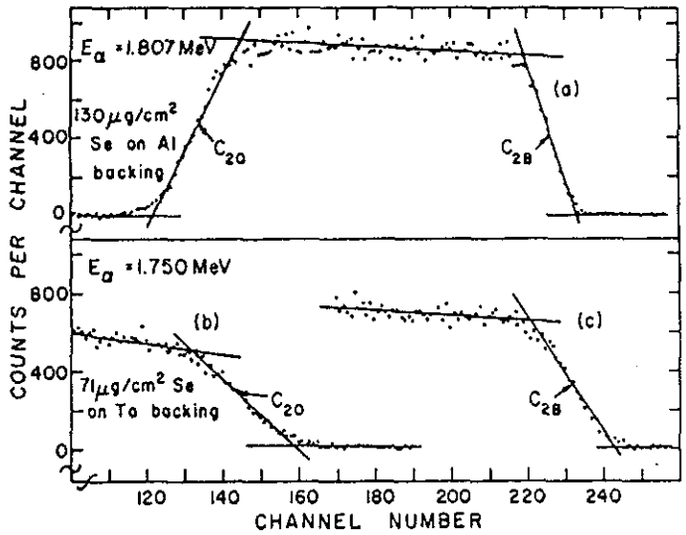

FIG. 18. Energy spectra of α particles elastically scattered at $\theta = 130°$. The target orientation was so fixed that the directions along both incident and detected α particles were 25° with respect to the normal to the target surface. Spectrum (a) describes α-particle scattering by a selenium target film prepared on an aluminum backing. The channel numbers C_{2B} and C_{20}, that is, the midpoints of the indicated steps, correspond to scattering from, respectively, the front and back surfaces of the target film. Spectra (b) and (c) were taken at the bombarding energy $E_\alpha = 1.750$ MeV; they represent scattering from a clean tantalum blank and from another onto which selenium has been uniformly deposited. In this case, however, both C_{2B} and C_{20} correspond to scattering by tantalum atoms on the front surfaces of the respective blanks. From Lin *et al.* (1973).[54]

2.4.5. Backscattering Energy Loss

Backscattering is one of the most often used methods of determining energy loss in solid targets. For a thin film on a thick substrate, the energy of projectiles backscattered from the thin film surface, or from the substrate surface if no thin film is present, will differ from that of projectiles scattered from the same element at the interface. The difference is attributed to the energy loss in the incident and outgoing paths.

This method was developed by Warters[52] to find the stopping cross section of protons in lithium. Several others have used it (see, for example, Chu and Powers[53] and Lin *et al.*[54]).

As an example, Fig. 18 from Lin *et al.*[54] shows energy spectra of helium ions elastically scattered at $\theta = 130°$. Spectrum (a) describes helium ion scattering by a selenium target film prepared on an aluminum backing. The channel numbers C_{2B} and C_{20}, that is, the midpoints of the indicated steps, correspond to scattering from, respectively, the front and back surfaces of the selenium target film. Spectra (b) and (c) were taken at the bombarding energy $E_\alpha = 1.750$ MeV; they represent scattering from a clean tantalum substrate and from tantalum onto which selenium has been uniformly deposited. For both cases the difference between C_{2B} and C_{20} represents the energy loss in the incoming path, and that in the outgoing after backscattering at the interface. An independent measurement of film thickness $\rho\,\Delta x$ by weighing provides the information on stopping cross sections.

Stopping cross sections measured by this method have experimental errors from ±2.2 to 3.3%. As an example, Fig. 19 shows Lin *et al.* mea-

[52] W. D. Warters, unpublished Ph.D. thesis, Calif. Inst. Tech., Pasadena (1953).
[53] W. K. Chu and D. Powers, *Phys. Rev.* 187, 478 (1969).
[54] W. K. Lin, H. G. Olson, and D. Powers, *Phys. Rev. B* 8, 1881 (1973).

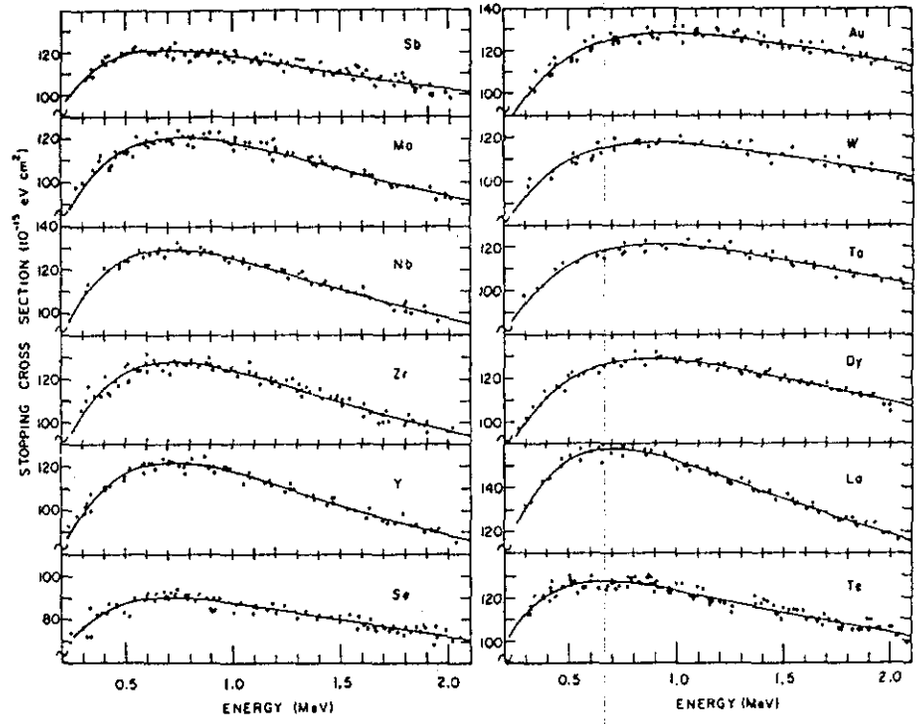

FIG. 19. Stopping cross sections of α particles vs. energy in Se, Y, Zr, Nb, Mo, Sb, Te, La, Dy, Ta, W, and Au. The experimental error ranges from ±2.2 to 3.3% of the average stopping cross section for the corresponding element. The solid curves were calculated from Brice's formula. For each element, these parameters were obtained individually by a least-squares fit of the data to the formula. From Lin *et al.* (1973).[54]

surements[54] of stopping cross sections of α particles vs. energy in Se, Y, Zr, Nb, Mo, Sb, Te, La, Dy, Ta, W, and Au. The solid curves are calculated values based on three parameters obtained individually by a least-squares fit of the data to Brice's formula.[38]

Lin *et al.* present their measurements, in addition to the data obtained earlier, in the plot of ϵ vs. Z_2 given in Fig. 20. The solid irregular curves are taken from a calculation, based on Lindhard's statistical approach, carried out by Rousseau *et al.*[41] and by Chu and Powers.[22,23] Measurements were made at stopping powers of 0.8 MeV (open symbols) and 2.0 MeV (closed symbols); the sources of the references are given by Lin *et al.*[54] As Fig. 20 shows, the experimental results for the periodic dependence of the Z_2 structure in stopping cross section are in good agreement with theoretical calculations. Figure 20 is also in good agreement with the findings presented in Fig. 7.

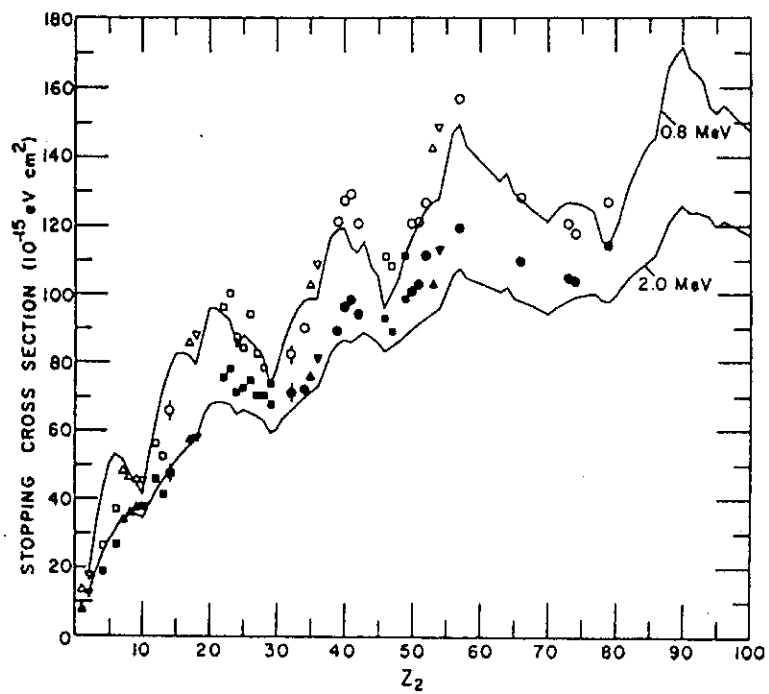

FIG. 20. α-Particle stopping cross section vs. the stopping-element atomic number Z_2 at 0.8 and 2.0 MeV. The solid curves are taken from the calculations, based on Lindhard's statistical approach, carried out by Rousseau *et al.* (1971).[41] Open and closed symbols, respectively, correspond to the 0.8- and 2.0-MeV data. From Lin *et al.*[54]

2.4.6. Backscattering Thick-Target Yield

All of the above-described methods of measuring energy loss involve measuring ΔE, an energy shift, and $N\,\Delta x$ or $\rho\,\Delta x$, the thickness of the target, which causes the energy shift. Therefore it is necessary to prepare a thin film and know its thickness. In this section, we describe a method that requires no thin-film target.

The thick-target yield method was first used by Wenzel and Whaling[55] in measuring the proton stopping cross section of ice. The method was later used in different manners, but the principle is always the same: the yield of elastic scattering of a projectile from a target is a function of the energy loss of the projectile in the target, before and after the scattering event.

As an example, Leminen[56] has measured the stopping power for protons in various metals by measuring the backscattering yield at the metal surface. Figure 21 shows his backscattering spectra of 500-keV protons elastically scattered from gold, tungsten, silver, molybdenum, copper, and titanium. The proton dose is 3 μC, and the scattering angle is 178°. The scattering yield is related to the scattering cross section, the solid angle of measurement, and the total number of protons incident on the target. The scattering yield at the surface is also related to the stopping cross sections at the incident energy and at scattered energies. A scattering yield measurement will produce energy loss information with probable error of about $\pm 3\%$. Leminen[56] used previously established stopping cross section data for copper, silver, and gold as his calibration standards in checking the internal consistency of his measurements. A similar principle has been applied by Feng *et al.*[57,58] to measure the relative stopping cross section ratio by measuring the spectrum height ratio at the interface of two layers.

These examples are measurements of backscattering yield at a well-defined energy, which corresponds to elastic scattering at the surface or the interface. By applying this method to the whole scattering yield spectrum, it should be possible to produce a curve of energy loss vs. energy. For example, Behrisch and Scherzer[59] assume the functional form of the stopping cross section to be $dE/dx = -AE^B$, where A and B are parameters. Since they also assume B to be 1/2, 0, or -1 for different energy regions, they can express energy loss analytically as a function of the

[55] W. A. Wenzel and W. Whaling, *Phys. Rev.* 87, 499 (1952).
[56] E. Leminen, *Ann. Acad. Sci. Fenn.*, Ser. A6, 386 (1972).
[57] J. S.-Y. Feng, W. K. Chu, and M.-A. Nicolet, *Thin Solid Films* 19, 227 (1973).
[58] J. S.-Y. Feng, W. K. Chu, and M.-A. Nicolet, *Phys. Rev. B* 10, 3781 (1974).
[59] R. Behrisch and B. M. U. Scherzer, *Thin Solid Films* 19, 247 (1973).

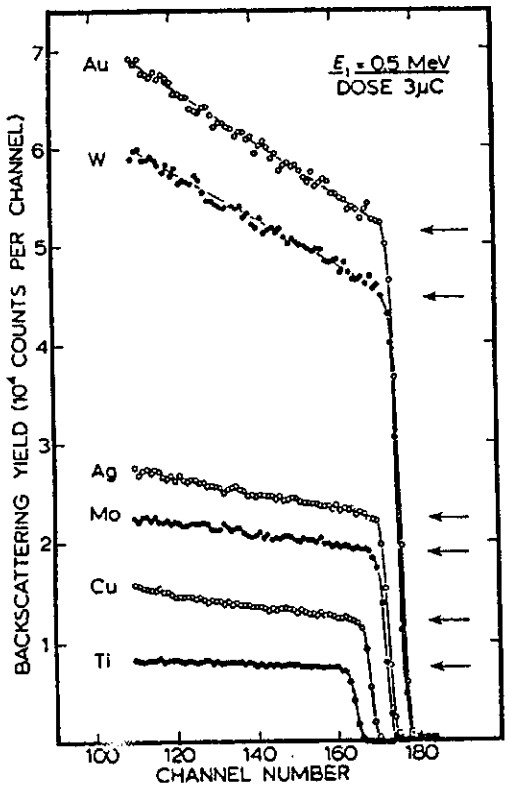

FIG. 21. Backscattering yield from Ti, Cu, Mo, Hg, W, and Au targets at a proton energy E = 500 keV. Proton dose is 3 μC. The arrows indicate the surface yield. From Leminen (1972).[58]

scattering yield at various energies. This enables them to translate a backscattering spectrum from a thick target into a curve of dE/dx vs. energy. Scherzer *et al.*[60] studied both methods, thick target and thin target, for energy loss of helium ions in gold. They list the approximations involved in both methods and the errors introduced by those approximations.

Lin *et al.*[61] have measured the stopping cross section of helium ions in gold and silver by the thick-target yield method. They use the stopping

[60] B. M. U. Scherzer, P. Børgesen, M.-A. Nicolet, and J. W. Mayer, *in* "Ion Beam Surface Layer Analysis" (O. Meyer, G. Linker, and F. Käppeler, eds.). Plenum Press, New York, 1976.

[61] W. K. Lin, S. Matteson, and D. Powers, *Phys. Rev. B* 10, 3746 (1974).

cross section ϵ expressed by three parameters n, a, and z, following Brice's formula:[38]

$$\epsilon = \frac{4\hbar^2}{5m}\frac{Z_1 + Z_2}{1 + (av/v_0)^n} \times \left[x^{1/2}\frac{30x^2 + 53x + 21}{3(x+1)^2} + (10x+1)\tan^{-1}x^{1/2}\right], \quad (2.4.10)$$

where $x = (v/2v_0z)^2$, $v_0 = e^2/\hbar$, v is the velocity of the α particles, and m is the electron mass. Three parameters n, a, and z, are obtained by a least-squares method that minimizes the difference between the measured backscattering yield spectrum and the calculated backscattering spectrum by using Eq. (2.4.10) and its relation to the thick-target yield. As an example, Fig. 22 gives backscattering spectra for α particles from silver at three different incident energies. From these spectra (solid points) the three parameters are obtained by the variation method:

$$n = 3.10, \qquad a = 0.352, \qquad z = 2.32. \quad (2.4.11)$$

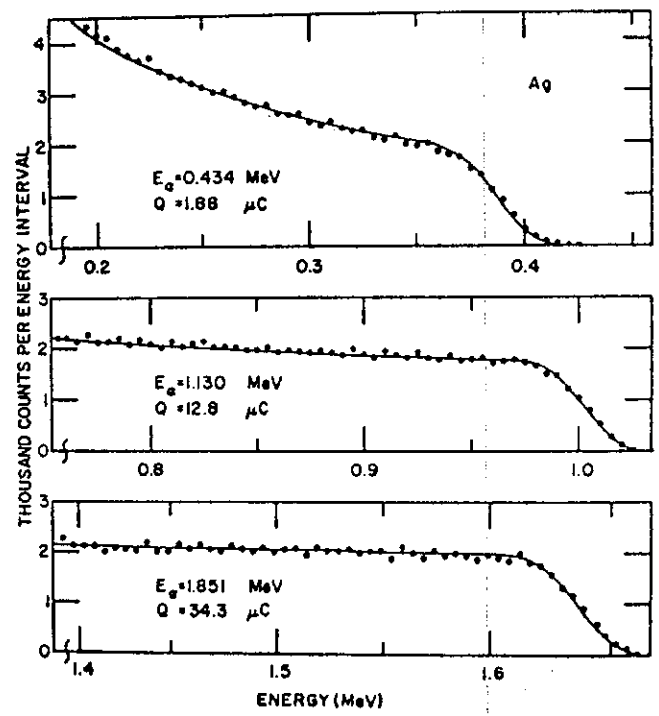

FIG. 22. Energy spectra from bombardment of α particles on thick mercury target. The curves were calculated from the stopping cross section of silver by use of Brice's formula. From Lin *et al.* (1974).[61]

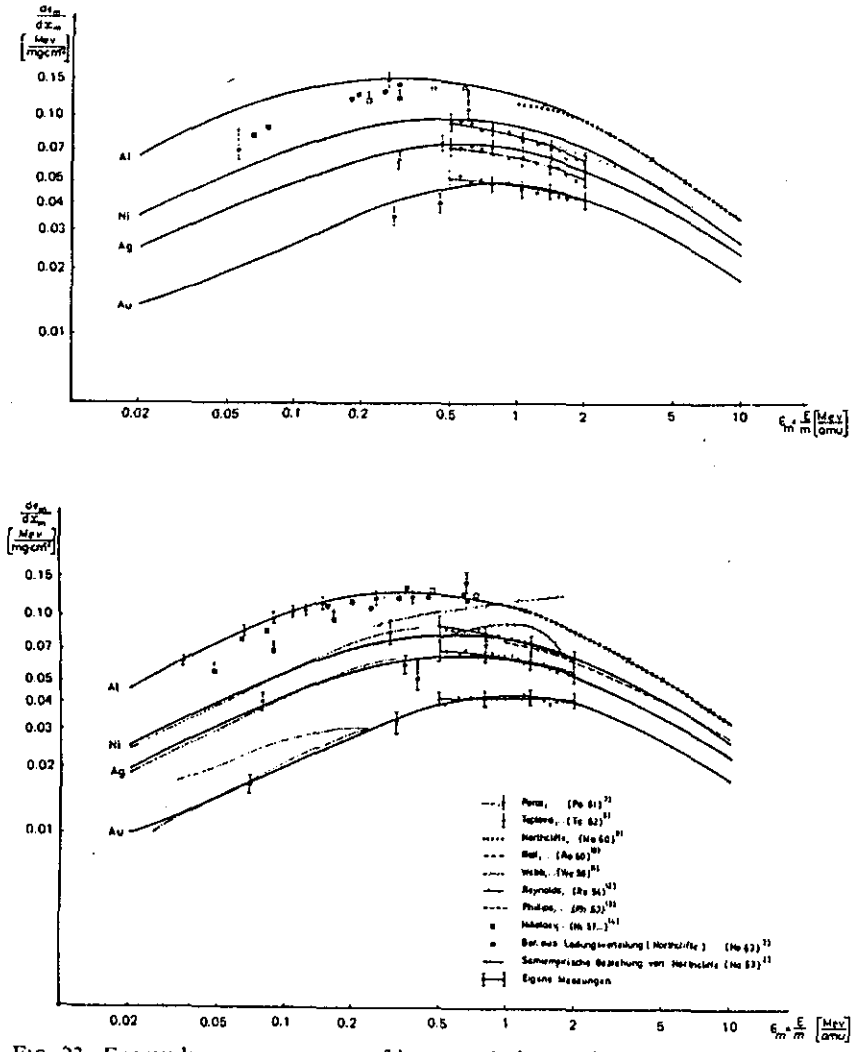

FIG. 23. Energy loss measurements of boron and nitrogen ions in metals by the thick-target yield method. From Bethge *et al.* (1966).[63]

By using this set of parameters, a calculated thick target yield curve can be obtained; it is shown as the solid curve in Fig. 21. The good agreement between the experimental spectra and the calculated ones provides a check of the thick-target yield method and shows that Brice's formula is an adequate expression of stopping cross section.

The thick-target yield method is not restricted to protons and helium

ions. Energy losses of boron, nitrogen, oxygen, and silicon ions in aluminum, nickel, silver, and gold have been measured by Bethge *et al.*[62,63] by a method based on the same principle. Their results for boron and nitrogen are illustrated in Fig. 23. Good agreement has been obtained between their measurements and earlier publications.

In general, the thick-target yield method is excellent for measuring energy loss. It avoids the difficulty of measuring the thickness of a thin film. However, the scattering cross section must be known; in all cases Rutherford scattering cross section is assumed to be valid in the application of the method. For an absolute measurement, accuracy in solid angle and current integration is crucial.

2.4.7. Measurement of Energy Loss by the Inverted Doppler Shift Attenuation (IDSA) Method

This experimental method for measuring energy loss is to some extent an inversion of the well-known Doppler shift attenuation (DSA) method for determining lifetime. For that method, dE/dx information is required. By inverting the problem, that is, knowing the lifetime of a γ-emitting reaction and measuring the Doppler shift attenuation of the γ ray, one can obtain information on dE/dx. This method has been described in several publications, such as Neuwirth *et al.*,[64] Hauser *et al.*,[65] and Latta and Scanlon.[66]

The γ-ray lifetime of an excited nuclear state can be measured by allowing a moving excited nucleus to slow down in some absorbing medium. The Doppler shift of the γ ray emitted is attenuated in a manner that depends on the lifetime of the γ-emitting state and on the slowing down (dE/dx) of the γ-emitting nuclei in the medium. Broude *et al.*[67] have found that apparently the lifetime value of a given ^{22}Ne state has an oscillatory dependence on the stopping medium Z_2. This dependence has been attributed to a nonsmooth dependence of the stopping power on Z_2. This Z_2 structure in the stopping cross section is predicted by Rousseau *et al.*,[41] on the basis of a Hartree–Fock–Slater atomic model that uses Lindhard and Winther's calculation. This demonstrates a potential for making accurate relative measurements of energy loss by inverting the DSA method.

[62] K. Bethege and P. Sandner, *Phys. Lett.* **19**, 241 (1965).
[63] K. Bethege, P. Sandner, and H. Schmidt, *Z. Naturforsch.* **21A**, 1052 (1966).
[64] W. Neuwirth, U. Hauser, and E. Kuehn, *Z. Phys.* **220**, 241 (1969).
[65] U. Hauser, W. Neuwirth, W. Pietsch, and K. Richter, *Z. Physik* **269**, 181 (1974).
[66] B. M. Latta and P. J. Scanlon, *Nucl. Instrum. Methods* **132**, 133 (1976).
[67] C. Broude, P. Englestein, M. Popp, and P. N. Tandon, *Phys. Lett. B* **39**, 185 (1972).

The stopping cross section ϵ is by definition connected with the differential energy loss along its path, that is,

$$\epsilon = \frac{1}{N}\frac{dE}{dx}, \tag{2.4.12}$$

since

$$E = \tfrac{1}{2}M_1 v^2, \tag{2.4.13}$$

$$\frac{dE}{dx} = \frac{dE}{dv}\frac{dv}{dx}, \tag{2.4.14}$$

$$\frac{dE}{dx} = M_1 v \frac{dv}{dx}. \tag{2.4.15}$$

Since $v = dx/dt$, Eq. (2.4.15) becomes

$$\frac{dE}{dx} = M_1 \frac{dv}{dt}, \tag{2.4.16}$$

and

$$\epsilon = \frac{M_1}{N}\frac{dv}{dt}, \tag{2.4.17}$$

if the atomic density N is known. This means that the energy loss, not ϵ, is related to the deceleration dv/dt, which can be derived from the slope of the Doppler spectrum. Therefore, the Doppler spectrum of an isotropically emitted γ ray is a direct measurement of the energy loss of the γ-emitting nucleus in its surrounding medium.

This method is very specific. It works only for a given nucleus that emits γ rays at a well-defined recoil energy. Therefore, it is not generally applicable to the problem of dE/dx. However, because it has high accuracy in measurements of relative stopping cross section, and because the study is for a specific ion at a well-defined energy region in various media, it is best applied when the target medium is the parameter. That means it is very powerful in applications of Bragg's rule—for example, in the work of Neuwirth *et al.*,[68] and also in the study of Z_2 structure in dE/dx by Pietsch *et al.*[69] as implied by Broude *et al.*[67]

As an example, we look at the study of energy loss of lithium in various media, using the IDSA method described by Hauser *et al.*[65] Nuclei of ^{7}Li* are produced from ^{10}B(n, α)^{7}Li* reaction. The asterisk indicates that ^{7}Li nuclei are in excited states and will emit γ rays for deexcitation. The

[68] W. Neuwirth, W. Pietsch, K. Richter, and U. Hauser, *Z. Phys. A* **275**, 209 (1975).
[69] W. Pietsch, U. Hauser, and W. Neuwirth, *Nucl. Instrum. Methods* **132**, 79 (1976).

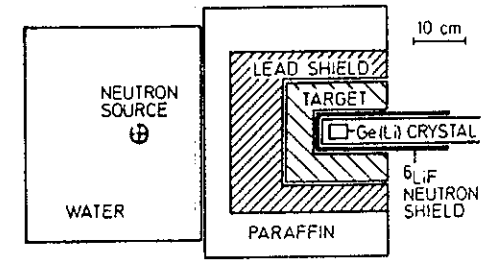

FIG. 24. Experimental setup for Doppler shift measurement. From Hauser *et al.* (1974).[65]

experimental setup is given in Fig. 24. The neutrons were produced by a 3-Ci americium–beryllium source. At this strength a given target material can be investigated over a period of one or two days. Water and/or paraffin are used as neutron moderators, so that the influx of neutrons into the target substance is isotropic. The target material has to contain ^{10}B in order to obtain ^{7}Li* from ^{10}B(n, α)^{7}Li reaction. Boron can be doped or implanted in a target of element Z_2 for the study of the ^{7}Li energy loss in Z_2. Boron can also be one of the elements in a compound for study of Bragg's rule, such as AlB_2, B_4C, B_2O_3, CrB_2, or B_4Si. The target medium can be in a solid, a liquid, or a gas.

In Fig. 24 a Ge(Li) detector is used in analyzing the energy of γ rays. A typical Ge(Li) detector will have a resolution of 1.3–1.6 keV (FWHM), which refers to the 477.55-keV γ rays emitted by ^{7}Li*. The γ-ray detector is shielded by ^{6}LiF to reduce neutron noise. The signal-to-noise ratio is proportional to the amount of ^{10}B content of the target. A typical γ-ray spectrum for the Doppler measurement is given in Fig. 25, where the target medium is CrB_2 and the detector resolution is 1.4 keV (FWHM). The reason for the broadening of the 477.55-keV γ ray is that the ^{7}Li is in motion, and so this is Doppler broadening. The shape of the broadening spectrum contains information on deceleration dv/dt, velocity, and the half-life of the nuclei emitting the γ rays. In other words, dv/dt can be written in terms of the half-life of the ^{7}Li*; the shape of γ-ray yield can be written as a function of the γ-ray energy and the velocity of ^{7}Li*. If we assume that the half-life of ^{7}Li* has been determined by another, independent method and by measuring the γ-ray yield vs. γ energy, the deceleration dv/dt vs. the velocity v of the ^{7}Li nuclei can be obtained, and energy loss vs. v for ^{7}Li is then obtained, in turn, by application of Eq. (2.4.16).

Neuwirth *et al.*[68] demonstrated this IDSA method in great detail in studies of the stopping cross section of ^{7}Li. A Z_2 oscillation found in their measurement can be predicted by calculations with a Hartree–Fock–Slater model. This is in good agreement with the Z_2 oscillation of ϵ for

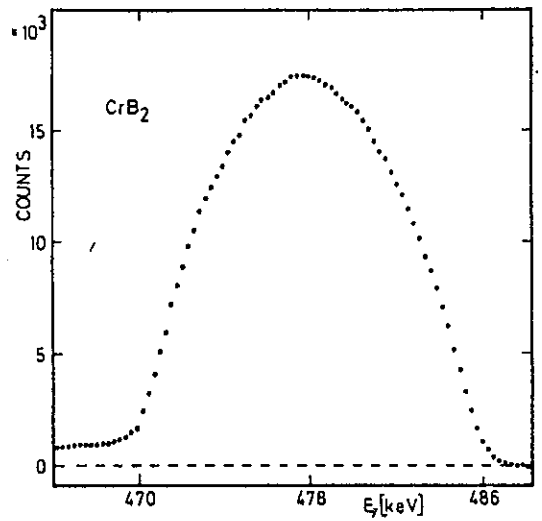

FIG. 25. Doppler spectrum of $^7Li^*$ stopped in CrB_2. Background is subtracted. From Hauser *et al.* (1974).[65]

^{4}He ions such as given in Figs. 7 and 20. Z_2 oscillations of ϵ for ^{14}N ions are measured and predicted in targets from carbon through molybdenum by Simons *et al.*,[70] and by Land and Brennan[71]; they have made range measurements of 800-keV $^{14}N^+$ in targets, using protons as probing projectiles, to induce $^{14}N(p,\gamma)^{15}O$ nuclear interaction. They then extract energy loss information from the range measurement.

The IDSA method, then, is a very powerful method for studying the target dependence of the stopping cross section. Because of its high relative accuracy, it is particularly useful in the study of Bragg's rule, Z_2 oscillation, and the physical state effect of heavy ions' stopping cross sections in media. One disadvantage is that the method applies only to a few specific nuclei in a given energy region.

2.5. Current Problems* in Stopping Cross Sections

Energy loss is one of the macroscopic properties of a target material. Its description involves only the Coulomb interaction between the projectile and the target electrons and nuclei. The study of the energy loss process has been one of the major sources of information on atomic physics, and recent applications of ion beams in various disciplines have brought a need for further study. Accurate measurements of energy loss are always in demand for studies of various effects and deviations from theories. Comprehensive theories that provide fairly accurate information on energy loss have been developed. We conclude this part by listing a few current problems related to dE/dx.

[70] D. G. Simons, D. J. Land, J. G. Brennan, and M. D. Brown, in "Ion Beam Surface Layer Analysis" (O. Meyer, G. Linker, and F. Käppeler, eds.). Plenum Press, New York 1976.

[71] D. J. Land and J. G. Brennan, *Nucl. Instrum. Methods* **132**, 89 (1976).

* See *Note Added in Proof* on p. 72.

2.5.1. Chemical Effect: Bragg's Rule

Bragg and Kleeman[72] first postulated the linear additivity of atomic stopping cross section. Because of its importance in radiation safety and health physics, the validity of this rule is constantly under test. For example, Powers *et al.*[73] have reviewed C–H and C–H–F compounds and found that there is a systematic deviation that depends on whether the compound is single-, double-, or triple-bonded. Neuwirth *et al.*[68,74] have shown that Bragg's rule is invalid for stopping cross sections of many metal–boron compounds for lithium ions of 80–800 keV. Deviations from Bragg's rule by up to 40% have been observed. Feng *et al.*[57,58] have found that Bragg's rule applies to metal alloys but not to metal oxides.

2.5.2. Solid-State Effect

A possible reason why Bragg's rule is invalid for a metal oxide is that the oxygen present in the metal oxide is in the solid phase rather than in the gaseous phase, according to Ziegler *et al.*,[75,76] who have given empirical corrections to the solid-state effect. That effect has also been calculated by Latta and Scanlon[77] and by Chu *et al.*[78] Both calculations indicate that the physical state of the stopping medium does exert a small effect on stopping cross sections. Recently Matteson *et al.*,[79] after reviewing and measuring the stopping cross section of helium ions in water vapor and in ice, observed that it is greater in vapor. Chu *et al.*[80] have measured

[72] W. H. Bragg and R. Kleeman, *Phil. Mag.* **10**, S318 (1905).

[73] D. Powers, A. S. Lodhi, W. K. Lin, and H. L. Cox, *Thin Solid Films* **19**, 205 (1973).

[74] W. Neuwirth, W. Pietsch, and R. Kreutz, *3rd Int. Conf. Ion Beam Anal.*, Washington, D.C. (1977).

[75] J. F. Ziegler, W. K. Chu, and J. S.-Y. Feng, *Appl. Phys. Lett.* **27**, 387 (1975).

[76] J. F. Ziegler and W. K. Chu, *J. Appl. Phys.* **47**, 2239 (1976).

[77] B. M. Latta and P. J. Scanlon, *Phys. Rev. A* **12**, 34 (1975).

[78] W. K. Chu, V. L. Moruzzi, and J. F. Ziegler, *J. Appl. Phys.* **46**, 2817 (1975).

[79] S. Matteson, D. Powers, and E. K. L. Chau, *Phys. Rev. A* **15**, 856 (1977).

[80] W. K. Chu, M. Braun, J. A. Davies, N. Matsunami, and D. A. Thompson, *3rd Int. Conf. Ion Beam Anal.*, Washington, D.C. (1977).

energy loss of helium ions in solidified oxygen, argon, and CO_2. Their results indicate that above 1 MeV, the energy loss differs only slightly in the gaseous phase and the solid phase; the maximum energy loss, however, occurs at somewhat higher energy in the solid phase. In the energy region below 1 MeV, the stopping cross sections of helium ions are about 5% lower than those reported for the corresponding gas.

2.5.3. Structure Effect

Softky[81] has found that the stopping cross section of protons of 1 MeV is 6% higher in graphite than in diamond. Matteson *et al.*[82] have found that the energy loss of 0.3–2-MeV α particles in graphite is 6–28% higher than the corresponding value for vapor-deposited carbon. They attributed the difference to an allotropic effect. For a single crystal, of course, the energy loss in a channeled direction is quite different from that in a random direction. Whether energy loss in a polycrystalline structure is or is not the same as that in an amorphous material of the same composition is not known; tests are being made to find out.

All the above three effects on the electronic stopping cross section are related to the slight change of outer-shell electronic configuration for a given element, either in a compound form or in a different phase or structure. They can therefore be considered basically the same, and an understanding of one will help in understanding the others.

2.5.4. Energy Straggling

Energy loss is a statistical process. The energy loss distribution is called energy straggling. A recent theory by Sigmund[83] indicates that correlation of target atoms in molecular gases causes an increase in straggling, and in addition to that, charge fluctuations of the projectile also give rise to an increase in straggling. Recent measurements by Besenbacher *et al.*[84] seem to confirm this theory. Measurements by Hvelplund[85] on low-energy helium ions having more energy straggling in N_2 gas than in neon can also be explained by this correlation effect proposed by Sigmund. Chu,[86] however, has interpreted Hvelplund's result with respect

[81] S. D. Softky, *Phys. Rev.* **123**, 1685 (1961).
[82] S. Matteson, E. K. ... Chau, and D. Powers, *Phys. Rev. A* **14**, 169 (1976).
[83] P. Sigmund, *Phys. Rev. A* **14**, 996 (1976).
[84] F. Besenbacher, J. Heinemeier, P. Hvelplund, and H. Knudsen, *Phys. Lett.* **61A**, 75 (1977).
[85] P. Hvelplund, *K. Dan. Vidensk. Selsk. Mat. Fys. Medd.* **38**, No. 4 (1971).
[86] W. K. Chu, *Phys. Rev. A* **13**, 2057 (1976).

to a Z_2 oscillation calculation of energy straggling. More straggling experiments are needed to verify some of the effects discussed here.

2.5.5. Charge State of the Projectiles

This subject is discussed in Part 6 by Macdonald. Because it is closely related to the energy loss of heavy ions, theoretical and experimental work on it will be important to information on the stopping cross section. So far there has been no direct experimental measurement of the charge state of a projectile *inside* a solid.

2.5.6. The Barkas Effect

The Barkas effect is the difference in the stopping of swift positive and negative particles. In Bethe's formula [Eq. (2.3.19)], the electronic stopping cross section derived by quantum perturbation theory to the first order gives the relation that the stopping cross section is proportional to Z_1^2. The Barkas effect could be explained by an extra term of order Z_1^3, which will yield a different stopping cross section according to whether Z_1 is positive or negative. Ashley *et al.*[87,88] have performed a classical perturbation calculation concerning a harmonic oscillator. The motion of the target electrons in the force field of the point charge projectile is treated up to quadratic terms in Z_1. Lindhard[89] has briefly reviewed the Barkas effect, and the higher-order effects. He approaches the problem from a simple classical Rutherford scattering from a screened potential. The Z_1^3correction given by Lindhard is about twice that given by Ashley *et al.* The Z_1^3, Z_1^4 effect has been verified in a few experiments.

2.5.7. Ion Clusters Effect

When the projectiles are ion clusters rather than individual ions, the mode of propagation is influenced by the ions within the medium, by the ion–ion interaction in the cluster through the wakes trailing each ion, and by the Coulomb repulsion between the ions. Those correlations complicate the motion of the projectiles in condensed medium, and make the energy loss greater than for a single ion. The energy loss of the ion cluster depends on the *partition* of the energy loss between single electron collision and resonant excitations in the target. Careful measurements of the stopping cross sections of correlated clusters and individual ions provide

[87] J. C. Ashley, W. Brandt, and R. H. Ritchie, *Phys. Rev. B* **5**, 2393 (1972).
[88] J. C. Ashley, W. Brandt, and R. H. Ritchie, *Phys. Rev. A* **8**, 2402 (1973).
[89] J. Lindhard, *Nucl. Instrum. Methods* **132**, 1 (1976).

information on this partition relation. A recent review is given by Brandt and Ritchie.[90]

2.5.8. Nuclear Energy Loss

For very low-energy heavy ions the nuclear energy loss is totally dependent on the interacting potential. Recent experimental results in low-energy ion implantation indicate that projected ranges calculated by the LSS theory are off by as much as 100%. Nuclear stopping cross sections lower than those calculated by the LSS theory have been given recently by Kalbitzer *et al.*[37] and by Wilson *et al.*[38] (see Fig. 6). Interaction potentials need further experimental verification before accurate theory on nuclear energy loss for very low-energy heavy ions can be formulated.

Note Added in Proof

Much progress has been made recently in the topics covered in Chapter 2.5. For example, energy straggling, ion clusters effect, and the Barkas effect have received much theoretical and experimental attention. This detailed progress cannot be covered in this short part.

[90] W. Brandt and R. H. Ritchie, *Nucl. Instrum. Methods* **132**, 43 (1976).